

Identification and Characterization of a Novel Indoleamine 2,3-Dioxygenase 1 Protein Degradator for Glioblastoma

Lakshmi R. Bollu,[●] Prashant V. Bommi,[●] Paige J. Monsen, Lijie Zhai, Kristen L. Lauing, April Bell, Miri Kim, Erik Lodomersky, Xinyu Yang, Leonidas C. Plataniias, Daniela E. Matei, Marcelo G. Bonini, Hidayatullah G. Munshi, Rintaro Hashizume, Jennifer D. Wu, Bin Zhang, Charles David James, Peiwen Chen, Masha Kocherginsky, Craig Horbinski, Michael D. Cameron, Arabela A. Grigorescu, Bakhtiar Yamini, Rimas V. Lukas, Gary E. Schiltz,* and Derek A. Wainwright*

Cite This: *J. Med. Chem.* 2022, 65, 15642–15662

Read Online

ACCESS |



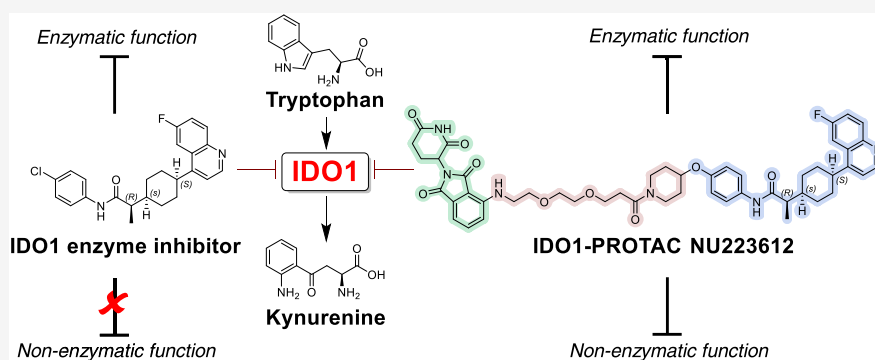
Metrics & More



Article Recommendations



Supporting Information



ABSTRACT: Indoleamine 2,3-dioxygenase 1 (IDO1) is a potent immunosuppressive enzyme that inhibits the antitumor immune response through both tryptophan metabolism and non-enzymatic functions. To date, most IDO1-targeted approaches have focused on inhibiting tryptophan metabolism. However, this class of drugs has failed to improve the overall survival of patients with cancer. Here, we developed and characterized proteolysis targeting chimeras (PROTACs) that degrade the IDO1 protein. IDO1-PROTACs were tested for their effects on IDO1 enzyme and non-enzyme activities. After screening a library of IDO1-PROTAC derivatives, a compound was identified that potently degraded the IDO1 protein through cereblon-mediated proteasomal degradation. The IDO1-PROTAC: (i) inhibited IDO1 enzyme activity and IDO1-mediated NF- κ B phosphorylation in cultured human glioblastoma (GBM) cells, (ii) degraded the IDO1 protein within intracranial brain tumors in vivo, and (iii) mediated a survival benefit in mice with well-established brain tumors. This study identified and characterized a new IDO1 protein degrader with therapeutic potential for patients with glioblastoma.

INTRODUCTION

Glioblastoma (GBM) is an aggressive primary brain tumor of adults and accounts for >50% of brain tumor-associated mortalities. The standard of care for a GBM patient includes surgical resection, followed by radiation and chemotherapy with temozolomide.¹ Despite the aggressive treatment strategy, the overall 5 year survival rate remains at only 5–15%.² Over the past 15 years, immune checkpoint blockade (ICB) has revolutionized cancer treatment by providing durable survival responses in patients with different cancer types. In contrast, ICB treatment has yet to confer an overall survival benefit to GBM patients in accordance with phase III clinical trial outcomes to date.^{3–6}

Indoleamine 2,3-dioxygenase 1 (IDO1) is an immunosuppressive enzyme that converts the essential amino acid tryptophan (Trp) into downstream metabolites referred to as

kynurenines (Kyn).^{7–10} IDO1 is expressed in a wide variety of human cancers, including GBM, and higher expression is inversely associated with patient survival.^{11–16} Thus far, treatment with an IDO1 enzyme inhibitor has failed to provide a survival benefit to human patients with cancer.¹⁰ This may be due to the ability of IDO1-expressing cancer cells to suppress the immune response through non-enzyme-mediated immunosuppressive functions.^{11,17–20} Specifically, mice with intracranial glioma cells expressing the catalytically inactive mutant IDO1

Received: May 19, 2022

Published: November 21, 2022



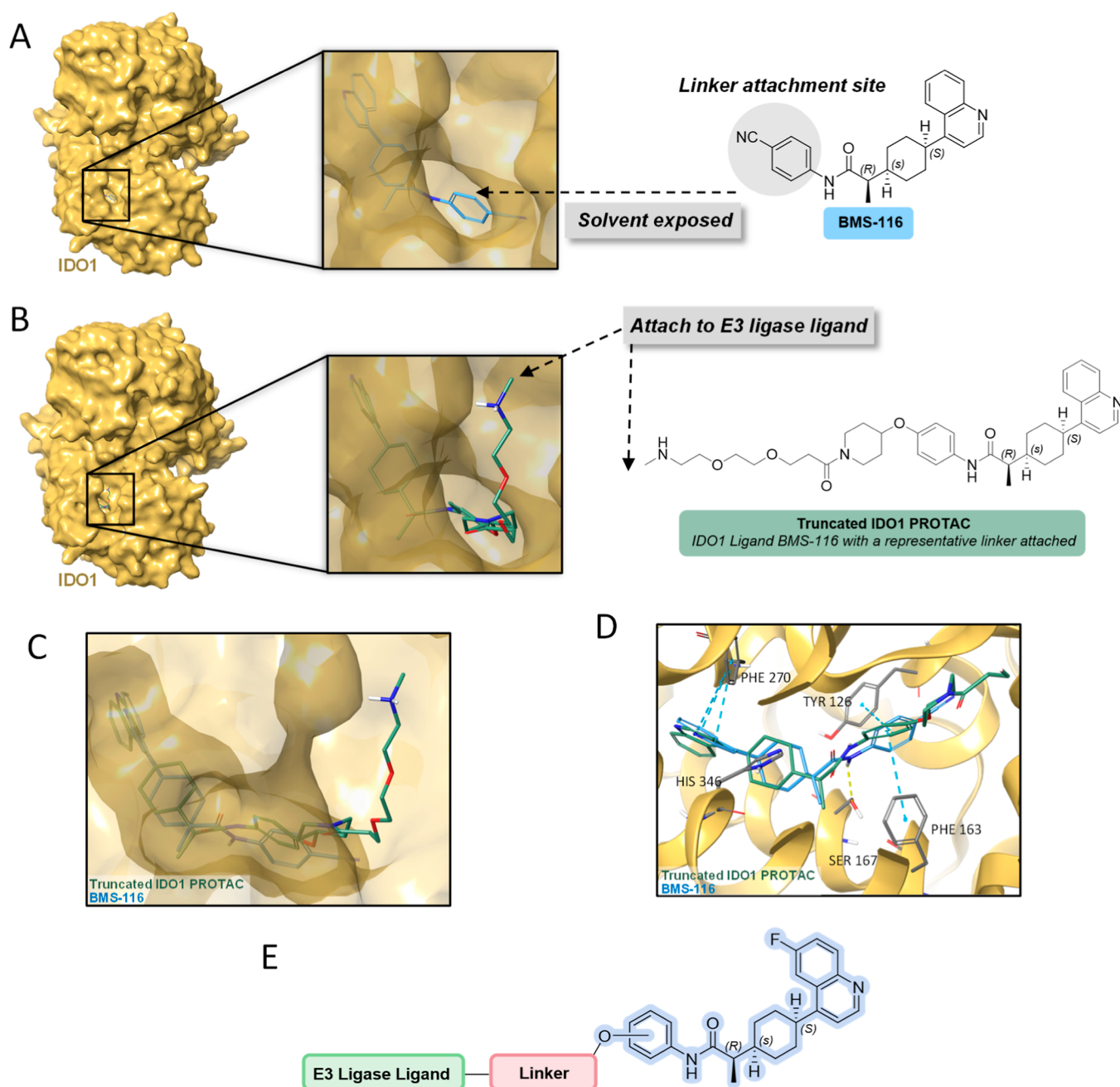


Figure 1. Design strategy of IDO1-PROTACs. (A) The co-crystal structure of IDO1 (gold, PDB: 6AZW) with the ligand BMS-116 (blue). (B) Docking model of BMS-116 with a representative linker attached (green). (C) and (D) Overlay of ligand BMS-116 (blue) with truncated IDO1-PROTAC (green) in the IDO1 active site with representative interactions. (E) General structural design of the IDO1-PROTAC library.

through substitution of histidine to alanine at the 350th amino acid had a similarly decreased survival rate as compared to mice with intracranial glioma cells expressing wild-type enzymatically active IDO1.¹⁷ The recent discovery that IDO1 suppresses anti-tumor immunity through a mechanism that extends beyond the canonical tryptophan metabolic effects motivated us to develop a new class of small molecules that inhibit both enzymatic and non-enzymatic activities. The aim of these new compounds is to fully inhibit IDO1-mediated immune suppression in subjects with cancer.^{9,20}

Proteolysis targeting chimera (PROTAC) technology has emerged as a promising new therapeutic approach for targeting non-druggable proteins that contribute to human diseases.^{21–23} PROTACs utilize an E3 ligase complex to ubiquitinate a protein

of interest and target it for proteasome-mediated degradation. Here, we report the development and characterization of a novel, potent IDO1-PROTAC that degrades the IDO1 protein in human GBM cells and mediates a therapeutic survival benefit in mice engrafted with a well-established brain tumor.

RESULTS

IDO1-PROTAC Library Design. Among the many IDO1 enzyme inhibitors developed to date, BMS-986205 (Linrodostat) was chosen to be utilized as the IDO1-binding ligand in the PROTAC design.²⁴ BMS-986205 is a selective, potent inhibitor for IDO1 with a cellular IC₅₀ of 0.5 nM and is orally bioavailable.²⁴ Furthermore, the availability of an IDO1-bound crystal structure with a BMS-986205 analogue (BMS-116)²⁴

allowed for the design of a suitable exit vector. Analysis of the co-crystal structure of IDO1 in complex with BMS-116 reveals the phenyl group is near an opening that can access the solvent, whereas the rest of the molecule is buried deeper within the active-site pocket (Figure 1A). Therefore, the phenyl ring would be a suitable anchor for the attachment of linkers.²⁴ To support this premise, we performed docking studies on a modified structure of BMS-116 in which a representative linker moiety was attached to the BMS-116 ligand (Figure 1B). According to this docked pose, the terminal amine on the linker group extends out of the active-site binding pocket and is exposed on the protein surface to the solvent. The BMS-116 ligand and the truncated IDO1-PROTAC participate in similar interactions in the binding pocket, suggesting that the designed IDO1-PROTACs may bind comparably (Figure 1C,D). Thus, the IDO1-PROTACs were designed by connecting various linker moieties to the phenyl group of the parental IDO1 inhibitor, BMS-986205 (Figure 1E).

In an effort to establish structure–activity relationship (SAR) data around the BMS-986205-derived PROTAC series and to maximize the likelihood of identifying a potent IDO1 degrader, we employed a strategy to design an IDO1-PROTAC library that involved three key points of diversification. These included the connection to the IDO1 binding ligand, the length/chemical composition of the linker, and the type of E3 binding ligand (Figure 1E). The connection of various linker structures to either the aryl 3- or 4-positions of the phenyl propanamide group of the parental IDO1 ligand via an ether attachment was evaluated. Linkers were explored with multiple lengths of polyethylene glycol (PEG) or alkyl chains and were connected to the E3 binding ligands via an amine, ether, or oxyacetamide attachment. In addition, some analogs contained a heterocyclic spacer group between the PEG/alkyl chains and the IDO1 binding ligand to increase structural rigidity. The cereblon (CRBN)-binding thalidomide ligand was used as the E3-binding ligand along with two variations of Von Hippel-Lindau (VHL)-binding ligands. Following the design strategy outlined in Figure 1, a library of approximately 100 IDO1-PROTAC compounds was generated.

Chemical Synthesis. To serve as a control, the parental IDO1 inhibitor, NU223618 (BMS-986205; Linrodostat), was synthesized through coupling carboxylic acid **1** with 4-chloroaniline to provide the desired IDO1 inhibitor (**2**, NU223618) with 86% yield (Scheme 1).

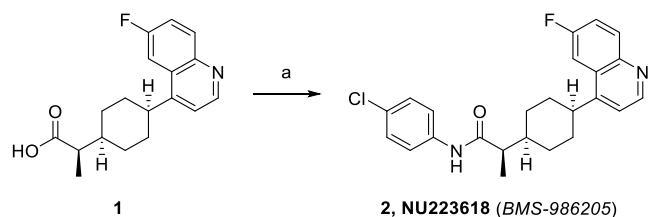
The synthetic route for NU223612 first involved functionalizing the IDO1-targeting ligand with piperidine attached through an ether bond (Scheme 2). The nucleophilic aromatic substitution reaction of commercially available 1-fluoro-4-nitrobenzene (**3**) with 1-boc-4-hydroxypiperidine in the

presence of potassium *tert*-butoxide furnished intermediate **4** in 86% yield. Subsequent reduction of the aryl nitro via catalytic hydrogenation using palladium on carbon afforded aryl amine **5** in high yield (88%). Amide coupling with carboxylic acid **1** using EDCI gave the amide (95% yield), followed by acid-mediated Boc-removal, which provided key intermediate **6** in a 97% yield. Functionalization of the CRBN-binding ligand began with nucleophilic aromatic substitution between 4-fluoro-thalidomide (**7**) and amino-PEG2-acid-*tert*-butyl ester to yield **9** in 14% yield (Scheme 2). Upon removal of the *tert*-butyl group to afford carboxylic acid **11** (83% yield), the desired E3-ligand containing coupling partner was reacted with amine **6** to yield the desired IDO1-PROTAC NU223612 (**13**) in 42% yield. A derivative of degrader NU223612 that contains a methyl group on the thalidomide which prevents binding to E3 ligase CRBN was prepared for use as a negative control. Methylation of the imide nitrogen of **7** with iodomethane afforded **8** in 73% yield (Scheme 2). Following similar synthetic transformations as above, nucleophilic aromatic substitution yielded **10** (26%) and acid-mediated removal of the *tert*-butyl group provided carboxylic acid **12** in 83% yield. Amide coupling between the newly formed acid **12** and amine **6** afforded the N-methylated IDO1-PROTAC, NU226211 (**14**), in 48% yield.

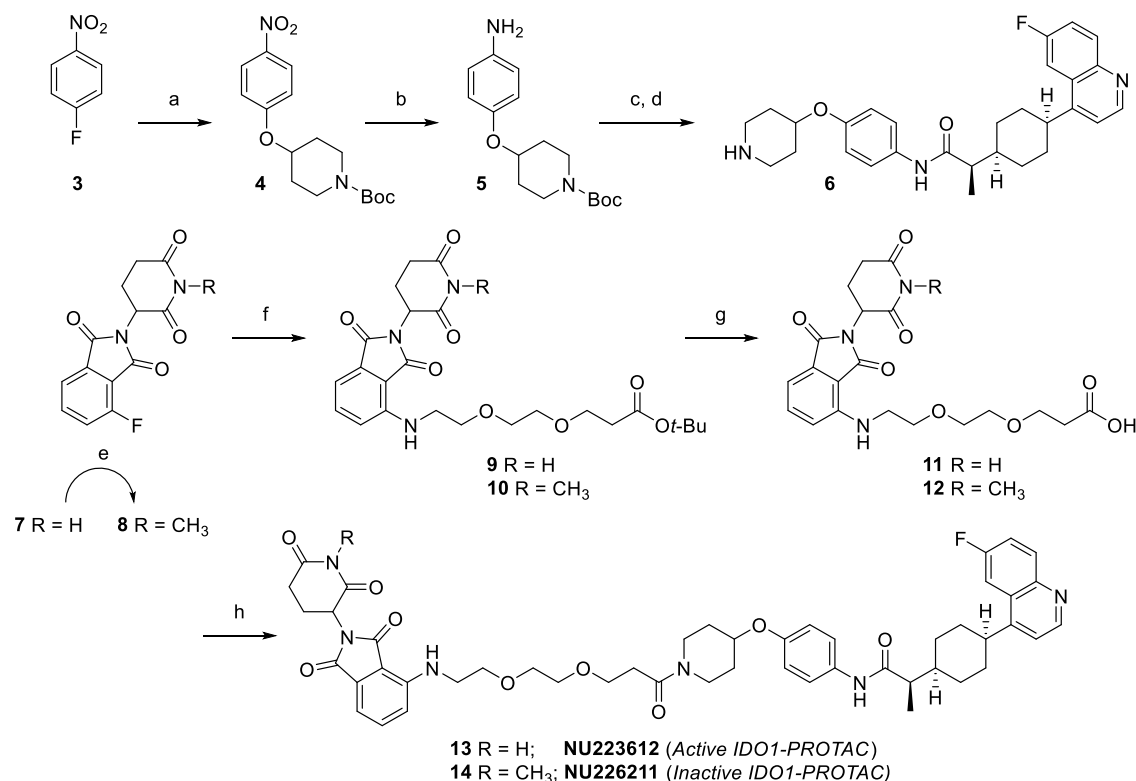
Structure–Activity Relationships of the IDO1-PROTAC Library. In an effort to identify a potent, effective IDO1 degrader, a library of around 100 diverse PROTACs was synthesized in a systematic approach (see Supporting Information for detailed synthetic procedures). SAR analysis of the PROTACs after evaluation for IDO1 degradation potential revealed that specific structural components are preferential for the activity of the IDO1-PROTAC (Tables 1, 2 and 3). Both CRBN and VHL-type ligands were identified to be suitable E3 ligase ligands for the degradation of IDO1. The VHL type II ligand, connected to the linker scaffold at the phenyl ring and containing a cyclopropyl group and an α -fluorine atom, was found to be superior to the VHL type I ligand. The VHL type II ligand has been shown to have increased binding affinity, cellular potency, and cell membrane permeability as compared to the VHL type I ligand, which may contribute to a more potent IDO1 degrader.²⁵ Furthermore, we designed a greater number of CRBN-based PROTACs based on the hypothesis that they would have better pharmacokinetic (PK) profiles and higher blood-brain barrier (BBB) penetration due to their smaller molecular weights and lower number of rotatable bonds and hydrogen bond donors.²⁶

It has become evident that the linker length and composition play key roles in the bioactivity and physicochemical properties of a PROTAC.²⁷ The linker is crucial for assisting in the spatial orientation and positioning of the E3 ligase and the protein of interest to ensure favorable protein–protein interactions (PPIs), a key element in the formation of a productive ternary complex.²⁸ Since alkyl and PEG chains are the most common linker motifs incorporated in PROTAC design, we chose to synthesize the IDO1-PROTACs with various alkyl and PEG chain lengths (3–17 atoms). Not surprisingly, the composition of the linker played a critical role in the potency of the IDO1-PROTAC. The utilization of a PEG linker was found to be more favorable than an alkyl linker chain, suggesting that linkers with a higher polarity may be favored over lipophilic chains. Additionally, the SAR data suggest that the length of the linker does contribute to IDO1-PROTAC activity. Shorter linker chains (<10 atoms) were substantially preferred over longer chains, as evidenced by a significantly larger percentage of top IDO1

Scheme 1. Synthesis of Parental IDO1 Ligand NU223618 (2, BMS-986205; Linrodostat)^a



^aReagents and conditions: (a) 4-chloroaniline, pyridine, EDCI, 0 °C to rt, 12 h, 86%.

Scheme 2. Synthesis of Active IDO1-PROTAC NU223612 (13) and the Inactive Analog NU226211 (14)^a

^aReagents and conditions: (a) 1-Boc-4-hydroxypiperidine, *t*-BuOK, THF, 0 °C to rt, 12 h, 86%; (b) Pd/C, H₂ (g), MeOH, rt, 6 h, 88%; (c) 1, EDCI, pyridine, 0 °C to rt, 12 h, 95%; (d) 4 N HCl in dioxane, rt, 12 h, 97%; (e) MeI, K₂CO₃, 0 °C to rt, 12 h, 73%; (f) R = H (7), amino-PEG2-acid-*tert*-butyl ester, DIPEA, DMF, rt to 80 °C, 12 h, 14%; R = CH₃ (8) amino-PEG2-acid-*tert*-butyl ester, DIPEA, DMF, rt, 12 h, 26%; (g) R = H (9), 4 N HCl in dioxane, rt, 6 h, 83%; R = CH₃ (10), 4 N HCl in dioxane, rt, 6 h, 83%; (h) R = H (11), 6, HATU, DIPEA, DMF, 0 °C to rt, 12 h, 42%; R = CH₃ (12), 6, HATU, DIPEA, DMF, 0 °C to rt, 12 h, 48%.

degraders having shorter linker units. This finding is unique for our class of IDO1-PROTACs as compared to the previously reported IDO1-PROTAC whereby a longer PEG-chain linker (23 atoms) was ideal.²⁹ This is not surprising since our IDO1-PROTACs contain BMS-986205 as the IDO1-targeting ligand, which is a heme-displacing inhibitor as compared to the heme-binding inhibitor, epacadostat.^{24,30} The difference in binding mode of the IDO1 inhibitor may affect the trajectory and optimal length of the linker motif. Various functional groups (amine, ether, oxycetamide) were employed as connecting units to the CRBN ligand and the inclusion of heterocyclic scaffolds (piperidine, azetidine) connecting the linker chain to the IDO1 ligand was investigated. Notably, altering the chemical composition of the attachment to the CRBN ligand, thalidomide, did not greatly influence effectiveness of the IDO1-PROTACs and is therefore a structural motif that can be further manipulated. Interestingly, the incorporation of a rigid heterocycle connecting the flexible linker chain to the IDO1-ligand appeared to be favorable. Specifically, the heterocyclic rings that are connected to the PEG chain via an amide bond, as portrayed in Tables 1–3, displayed significantly greater degradation of IDO1 in contrast to PROTACs lacking this structural feature. This observation suggests that the inclusion of a rigid scaffold connecting the linker to the IDO1 binding ligand may assist in the conformational restriction of the PROTAC, leading to enhanced PROTAC-protein interactions and/or PPIs. Additionally, the amide-connected heterocycles may interact with key residues in the IDO1 protein, assisting in the formation and stability of the ternary complex essential for

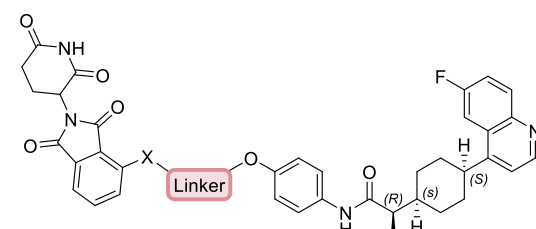
protein degradation. The final diversification of the IDO1-PROTACs explored was the *meta*- versus *para*-substitution to the IDO1-ligand. A high percentage of the top IDO1-PROTACs embodied the *para*-substitution to the IDO1-ligand, though further analysis and comparison of this structural modification are needed to draw a clearer conclusion. Overall, the SAR data obtained from testing the initial library of approximately 100 IDO1-PROTACs suggests that further derivatization of the linker and connectivity to both the E3 ligase ligand and IDO1 ligand can be explored. Additional analysis into the structural scaffolds that are ideal for IDO1 degradation is currently under investigation.

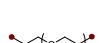
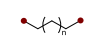
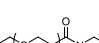

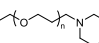
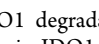

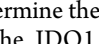
Characterization of the Lead Compound NU223612.

Each IDO1-PROTAC was tested by western blotting in U87 human glioblastoma cells pre-stimulated with 50 ng/mL interferon-gamma (IFN γ) according to the treatment scheme outlined in Figure 2A at a starting concentration of 10 μ M (Figure S1). Eighteen PROTACs from the initial IDO1-PROTAC library displaying a decrease in IDO1 protein levels at 10 μ M were further evaluated along with the parental IDO1 ligand, NU223618, across a dose range (0.1, 1, and 10 μ M) as summarized in the heatmap (Figure 2B). Western blotting identified NU223612 as the most potent compound, with significant IDO1 protein degradation observed at 100 nM (Figure S2A).

NU223612 was further evaluated in cultured U87 and human GBM43 cells followed by the quantification of IDO1 protein levels. NU223612 decreases IDO1 protein levels dose-dependently (Figure 2C,D). Western blotting analysis demonstrates

Table 1. CRBN-Type IDO1-PROTACs with Different Linker Structures and *Para*-Attachment to the IDO1 Ligand^a

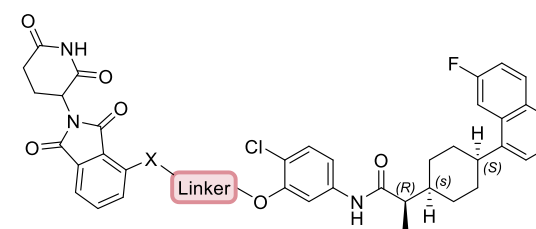


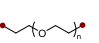
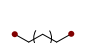
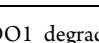
Linker	X	n	Compound ID	IDO1 Degradation (%) ^a
	NH	1	NU223599	23
		2	NU223602	77
		3	NU226132	0
		4	NU226181	0
		5	NU226186	0
	O	1	NU223600	18
		2	NU223603	94
		3	NU226133	0
		4	NU226182	0
		5	NU226187	0
	OCH ₂ CONH	1	NU223601	48
		2	NU223604	47
		3	NU226135	0
		4	NU226184	0
		5	NU226189	46
	NH	2	NU223605	0
		8	NU226180	0
	O	2	NU223606	0
		8	NU226137	0
	OCH ₂ CONH	2	NU223607	10
		5	NU223608	0
	NH	1	NU223610	33
		2	NU223612	94
	O	1	NU223609	45
		2	NU223613	80
	OCH ₂ CONH	1	NU223611	38
		2	NU223792	81
	NH	1	NU223805	90
		2	NU223807	94
	O	1	NU226151	86
		2	NU223808	74
	OCH ₂ CONH	1	NU223806	86
		2	NU223858	9
	O	1	NU226191	0
		2	NU226193	0
	OCH ₂ CONH	1	NU226154	66
		2	NU226155	33
	OCH ₂ CONH	2	NU226139	0

^aIDO1 degradation was measured in U87 cells using western blot analysis. IDO1 was induced in U87 cells with 50 ng/mL human IFN γ for 24 h, followed by a 10 μ M treatment of IDO1-PROTAC for 24 h before protein samples were prepared for western blotting analysis. Percent of normalized IDO1 protein levels were derived from densitometric analysis of band intensities.

that neither NU226211 nor NU223618 decreases IDO1 protein levels in GBM cells in vitro (Figure S2B,C). To determine the DC₅₀, the concentration of the drug at which 50% of the IDO1 protein is degraded, IFN γ -stimulated U87 and GBM43 cells were treated with various concentrations of NU223612, beginning with 0.01 μ M and increasing up to 30

Table 2. CRBN-Type IDO1-PROTACs with Different Linker Structures and *Meta*-Attachment to the IDO1 Ligand^a



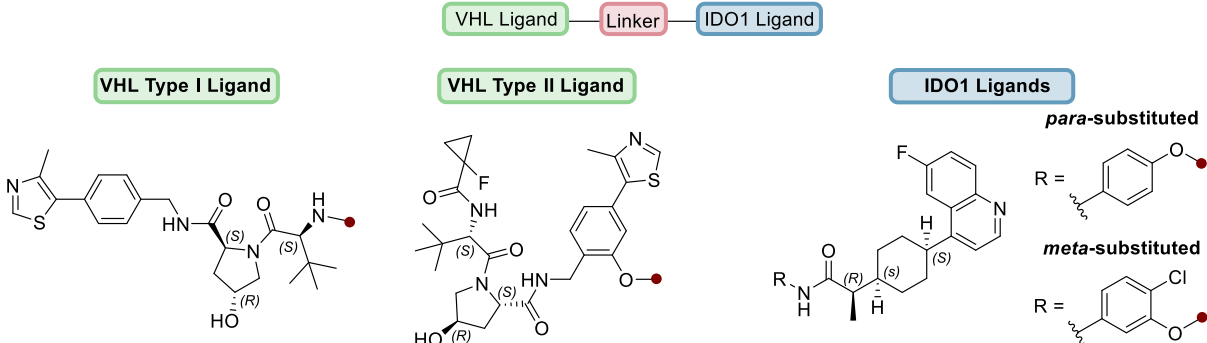
X	Linker	n	Compound ID	IDO1 Degradation (%) ^a
	NH	1	NU223793	66
		2	NU223795	71
		3	NU226140	0
		4	NU226195	0
		5	NU226145	0
	O	1	NU223616	6
		2	NU223617	88
		3	NU226141	13
		4	NU226196	0
		5	NU226146	0
	OCH ₂ CONH	1	NU223794	8
		2	NU223796	40
		3	NU226143	0
		4	NU226198	0
		5	NU226148	0
	NH	1	NU223813	36
		4	NU223814	0
		7	NU226156	0
	O	1	NU223614	49
		4	NU223615	0
	OCH ₂ CONH	7	NU223857	16
		1	NU223797	67
	OCH ₂ CONH	4	NU223798	0
		7	NU226157	0

^aIDO1 degradation was measured in U87 cells using western blot analysis. IDO1 was induced in U87 cells with 50 ng/mL human IFN γ for 24 h, followed by a 10 μ M treatment of IDO1-PROTAC for 24 h before protein samples were prepared for western blotting analysis. Percent of normalized IDO1 protein levels were derived from densitometric analysis of band intensities.

μ M (Figure 2E,G). A DC₅₀ of 0.3290 and 0.5438 μ M in U87 and GBM43 cells was determined, respectively (Figure 2F,G).

NU223612 Degrades IDO1 Protein in Multiple Cell Types. To assess the general ability of NU223612 to decrease intracellular IDO1 protein levels beyond that of human GBM cells, its activity was further analyzed in CD18 and PANC-1 human pancreatic cancer cells, OVCAR5 and SKOV3 human ovarian cancer cells, PC3 human prostate cancer cells, and the syngeneic GL261 mouse IDO1 cDNA-expressing (IDO1-O/E) glioma cell line.^{11,31} Consistent with the effects shown in Figure 2, NU223612 dose-dependently degrades IDO1 in all of the human cancer cell types that were analyzed (Figure S3A–F). NU223612 also degrades endogenous IDO1 protein in human GBM6 cells (Figure S3G), human pediatric DIPG KNS42 cells (Figure S3H), and DIPG007 neurosphere cell cultures (Figure S3I).

Since IDO1 can be expressed by non-tumor cells, including immune cells, and because IDO1-expressing immune cells have been shown to contribute to immune suppression,³² peripheral blood mononuclear cells (PBMCs) obtained from GBM and non-GBM patients were also treated with NU223612. As

Table 3. VHL-Type IDO1-PROTACs with Different Linker Structures and Connectivity to the IDO1 Ligand^a


Linker	IDO1 Ligand	VHL Type I Ligand			VHL Type II Ligand			
		n	Compound ID	IDO1 Degradation (%) ^a	n	Compound ID	IDO1 Degradation (%) ^a	
	<i>para</i>	1	NU223799	0	1	NU223801	39	
		2	NU223800	0	2	NU223802	0	
		3	NU226134	0	3	NU226136	0	
		4	NU226183	0	4	NU226185	0	
		5	NU226188	0	5	NU226190	27	
	<i>meta</i>	1	NU223809	0	1	NU223811	23	
		2	NU223810	0	2	NU223812	0	
		3	NU226142	0	3	NU226144	0	
		4	NU226197	0	4	NU226199	0	
		5	NU226147	0	5	NU226149	0	
	<i>para</i>	2	NU226178	0	2	NU223803	10	
		5	NU226179	0	5	NU223804	41	
		8	-	-	8	NU226150	23	
	<i>meta</i>	1	NU223854	0	1	NU223815	0	
		4	NU223855	21	4	NU223816	0	
		7	NU223856	3	7	NU223817	90	
		<i>para</i>	1	NU226152	88	1	NU223852	72
			2	NU226153	67	2	NU223853	3
<i>para</i>	-	-	-	1	NU223850	20		
	-	-	-	2	NU223851	91		
<i>para</i>	-	-	-	1	NU226192	0		
	-	-	-	2	NU226194	0		

^aIDO1 degradation was measured in U87 cells using western blot analysis. IDO1 was induced in U87 cells with 50 ng/mL human IFN γ for 24 h, followed by a 10 μ M treatment of IDO1-PROTAC for 24 h before protein samples were prepared for western blotting analysis. Percent of normalized IDO1 protein levels were derived from densitometric analysis of band intensities.

hypothesized, **NU223612**, but not **NU226211** nor **NU223618**, degrades IDO1 protein in GBM patient-isolated PBMCs (Figure S3J) as well as in PBMCs isolated from non-GBM patients (Figure S3K). Previously, we reported that tumor-infiltrating lymphocytes induce IDO1 expression in GBM cells. Therefore, we evaluated whether the IDO1-PROTAC degrades PBMC-induced human U87 GBM cell IDO1 protein expression. As shown in Figure S3L, **NU223612** mediated significant protein degradation of PBMC-induced IDO1 protein levels in U87 cells.

NU223612 was further analyzed for IDO1 degradation potential in U87 cells expressing IDO1-FLAG or -HA cDNA, and it was determined that the IDO1-PROTAC degrades the IDO1 protein in both IDO1-tagged cell lines (Figure S4A). Since IDO1 can localize both to the cytoplasm and to the nucleus of human GBM cells,¹² **NU223612** was also evaluated

for nuclear and cytoplasmic IDO1 degradation potential. As shown in Figure S4B, **NU223612** equally degraded IDO1 protein levels in both the cytoplasmic and nuclear intracellular compartments. We also investigated whether increased IDO1 protein levels affect IDO1-PROTAC effectiveness in human U87 cells that are stimulated with increasing levels of IDO1-inducing IFN γ concentrations. Although IDO1 protein levels plateau after treatment with ≥ 250 ng/mL IFN γ , the increased IDO1 expression did not affect the ability of **NU223612** to degrade IDO1 protein (Figure S4C). Thus, **NU223612** efficiently degrades a range of IDO1 protein levels and is able to penetrate subcellular compartments.

Recent studies from our group suggest that IDO1 non-enzyme-mediated functions contribute to GBM progression and escape from immune-mediated tumor control.¹⁷ To determine if the IDO1-PROTAC inhibits non-enzyme-dependent IDO1

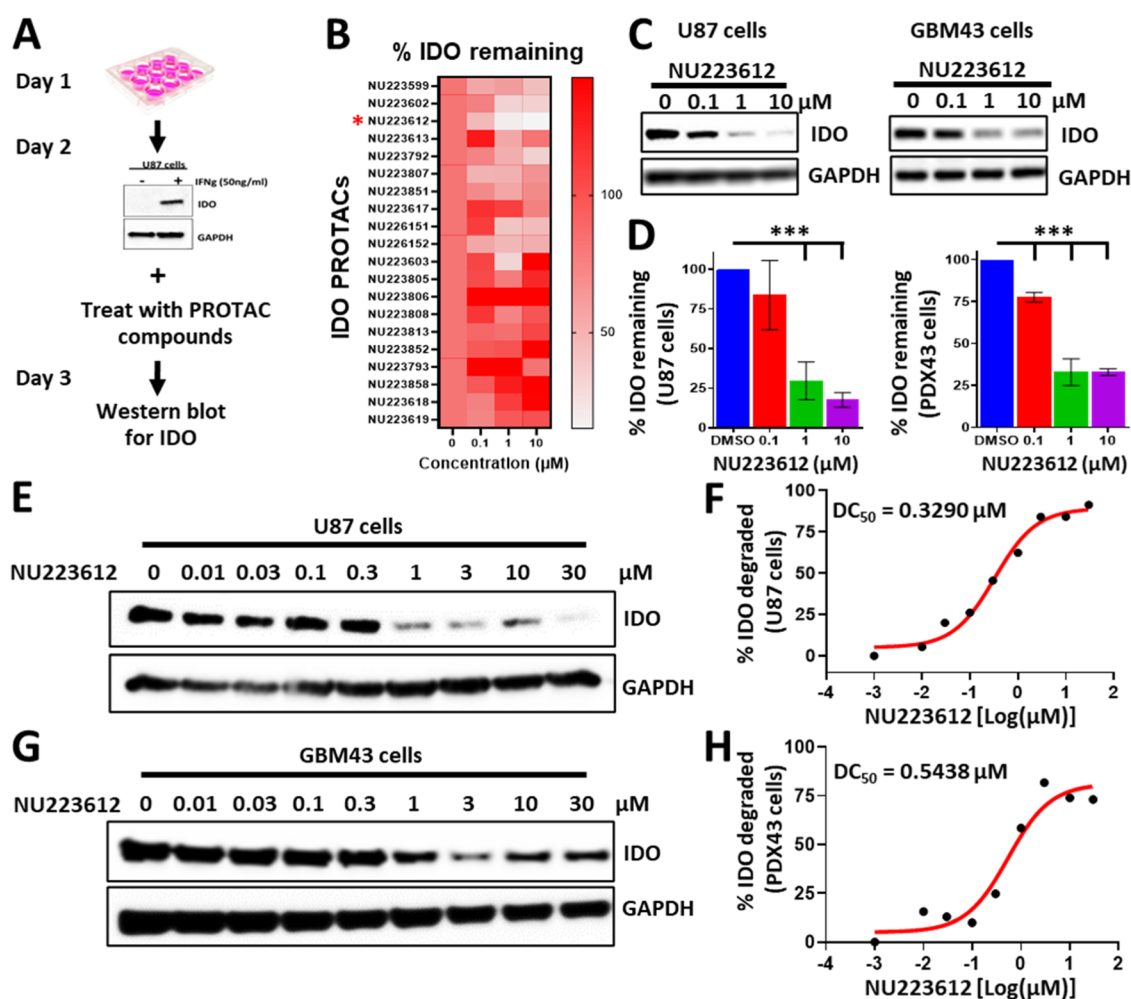


Figure 2. Discovery of a potent IDO1-PROTAC that promotes robust IDO1 protein degradation in human glioblastoma (GBM) cells. (A) Schema for screening IDO1-PROTAC compounds in human U87 GBM cells. (B) Heat map analysis to screen IDO1-PROTACs. Percent of IFN γ -induced IDO1 levels as normalized to untreated samples were calculated in U87 cells after treating with IDO1-PROTAC compounds at 0, 0.1, 1, and 10 μ M concentrations for 24 h (C) NU223612-induced IDO1 degradation in U87 and human GBM43 cells using western blot analysis. IDO1 was induced in U87 and GBM43 cells with 50 ng/mL human IFN γ for 24 h, followed by treatment with NU223612 for 24 h, before protein samples were prepared for western blotting analysis. (D) Percent of normalized IDO1 protein levels in U87 and GBM43 cells, derived from densitometric analysis of band intensities (from panel C), after treating with NU223612 for 24 h (E) U87 cells were treated with an extended dose range of NU223612 for 24 h, and protein samples were analyzed by western blotting. (F) Representative curve of percent IFN γ -induced IDO1 levels that were normalized to untreated samples as calculated in U87 cells (from panel E) to determine DC₅₀ that results in 50% of IDO1 degradation ($n = 3$ independent experiments). (G) GBM43 cells were treated with an extended dose range of NU223612 for 24 h, and protein samples were analyzed by western blotting. (H) Representative curve of percent IFN γ -induced IDO1 levels that were normalized to untreated samples as calculated in GBM43 cells (from panel G) to determine DC₅₀ that produces 50% of IDO1 degradation ($n = 3$ independent experiments). Data: mean \pm SEM. Statistical analysis: unpaired two-tailed Student's t -test. *** $P < 0.001$.

functions, NU223612 was evaluated against a catalytically inactive mutant IDO1 protein. NU223612 facilitated protein degradation of IDO1 enzyme-dead protein, similar to its effects on IDO1 wild-type protein (Figure S4D). Aside from IDO1, GBM cells constitutively express the tryptophan metabolic enzyme, tryptophan dioxygenase (TDO) 2.³³ In contrast to its effects on degrading IDO1, NU223612 did not decrease TDO2 protein levels confirming that its inhibitory effects on Kyn levels are IDO1-dependent and TDO2-independent (Figure S4E). The specificity of NU223612 is reflected in its ability to degrade IDO1, regardless of its tryptophan metabolic potential.

NU223612-Mediated Degradation of IDO1 Requires the Proteasome. The kinetics of IDO1-PROTAC-mediated protein degradation in human GBM cells were analyzed next. NU223612 began degrading the IDO1 protein at 16 h after treatment initiation and its effects lasted for at least 96 h (Figure

3A,B). A single continuous treatment with 1 and 10 μ M NU223612 degraded IDO1 protein levels for up to 72 h (Figure 3C). Interestingly, the complete withdrawal, or washout, of NU223612 after 24 h from culture media did not affect the degradation of IDO1 protein (Figure 3D), which suggests that the pharmacologic effects of NU223612 persist long after the initial administration.

U87 cells expressing FLAG-tagged-IDO1 cDNA were treated with NU223612, and the cell lysate was immunoprecipitated for IDO1. NU223612 causes monoubiquitination of IDO1 as compared to cells treated with DMSO (Figure 3E). Notably, neither NU226211 nor NU223618 mediated the ubiquitination of U87 cells that express the IDO1 protein. Treatment of U87 cells with the combination of NU223612 and the competitive IDO1 enzyme inhibitor NU223618 inhibits IDO1 degradation as compared to the treatment with NU223612 alone (Figure

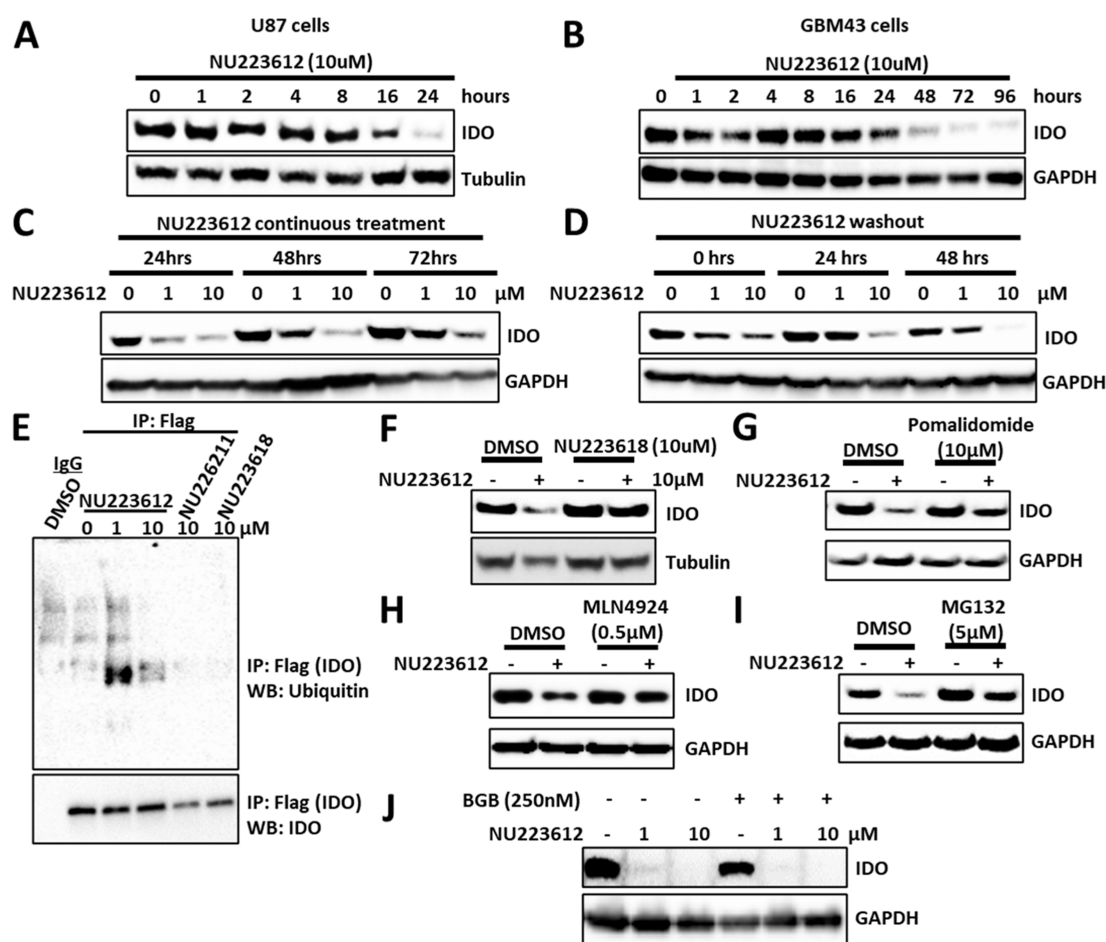


Figure 3. Characterization of NU223612 as a potent IDO1-PROTAC. (A,B) Western blot analysis of IDO1 and GAPDH to determine the kinetics of NU223612-induced IDO1 protein degradation in U87 and GBM43 cells, respectively. (C) Western blot analysis of IDO1 to determine the effect of a single continuous treatment of NU223612 on IDO1 protein levels at multiple time points in U87 cells. (D) Similar to (C), U87 cells were treated with NU223612 for 24 h, and cells were cultured without NU223612 for up to 48 h. Protein samples were tested in Western blot analysis to determine IDO1 levels upon withdrawal of the IDO1-PROTAC. (E) Western blotting analysis to determine IDO1 ubiquitination in immunoprecipitated samples isolated from U87 IDO1 FLAG cDNA-expressing cells after treating with NU223612, NU226211, or the parental compound, NU223618. Western blotting analysis of IDO1 and GAPDH to determine the effect of parental competitive IDO1-inhibitor (NU223618), (F) E3 ligase ligand (pomalidomide), (G) E1 ligase inhibitor (MLN4924), (H) proteasome inhibitor (MG132), (I) and non-competitive IDO1-inhibitor (BGB-7204) (J) on NU223612-induced IDO1 degradation.

3F). In contrast, co-incubation of NU223612 with the non-competitive IDO1 enzyme inhibitor, BGB-7204,^{31,34} failed to inhibit IDO1 protein degradation (Figures 3J; S5A). Similarly, the treatment with excess pomalidomide to prevent binding of NU223612 to CRBN (Figure 3G), the inhibition of E1-ligase activity using MLN4924 (Figure 3H), or the inhibition of proteasome activity with MG132 (Figure 3I), each result in the ablation of IDO1-PROTAC-mediated IDO1 protein degradation. These data confirm that NU223612 mediates IDO1 protein degradation through a ubiquitin-dependent proteasome-mediated degradation pathway.

NU223612/IDO1/CRBN Ternary Complex Formation.

To better understand how NU223612 decreases intracellular IDO1 protein levels, we characterized the binary and ternary complexes formed by NU223612 with recombinant IDO1 and CRBN proteins in vitro. Bio-layer interferometry (BLI) was used to measure the binding affinity (K_d) and kinetic parameters (k_{on} and k_{off}) of these complexes.^{35,36} All assays were performed at 30 °C in PBS with 0.5% DMSO. In the first set of experiments, NU223612, NU226211, and NU223618, each containing a similar BMS-986205-derived moiety, were confirmed to directly

bind to the IDO1 protein. The binding affinities of the three compounds to IDO1 were 640 nM, 1.1 μ M, and 470 nM, respectively (Figure 4A). Next, we examined the interaction of the three compounds with the CRBN ligase. NU223612 was bound to CRBN with an affinity of 290 nM. In contrast, no measurable binding to CRBN was detected for compounds NU223618 or NU226211 (Figure 4B). The affinity and selectivity of CRBN for NU223612 were also confirmed using isothermal calorimetry (ITC) assays (Figure S6A,B).

To detect and characterize the ternary NU223612/IDO1/CRBN complex, we followed a previously described procedure.³⁷ NU223612 was preincubated with a 25-fold molar excess of CRBN, and binding of the resulting NU223612/CRBN binary complex to IDO1 was detected and measured in real-time using BLI (Figure 4C). Binding sensorgrams collected data for a concentration series of either NU223612 alone (Figure 4D) or NU223612 pre-incubated with CRBN as shown in Figure 4. Since BLI is exquisitely sensitive to molecular size, the magnitude of the response signal differentiates between the binding of a protein-containing complex (CRBN-NU223612) and the binding of a small molecule (NU223612) alone. In

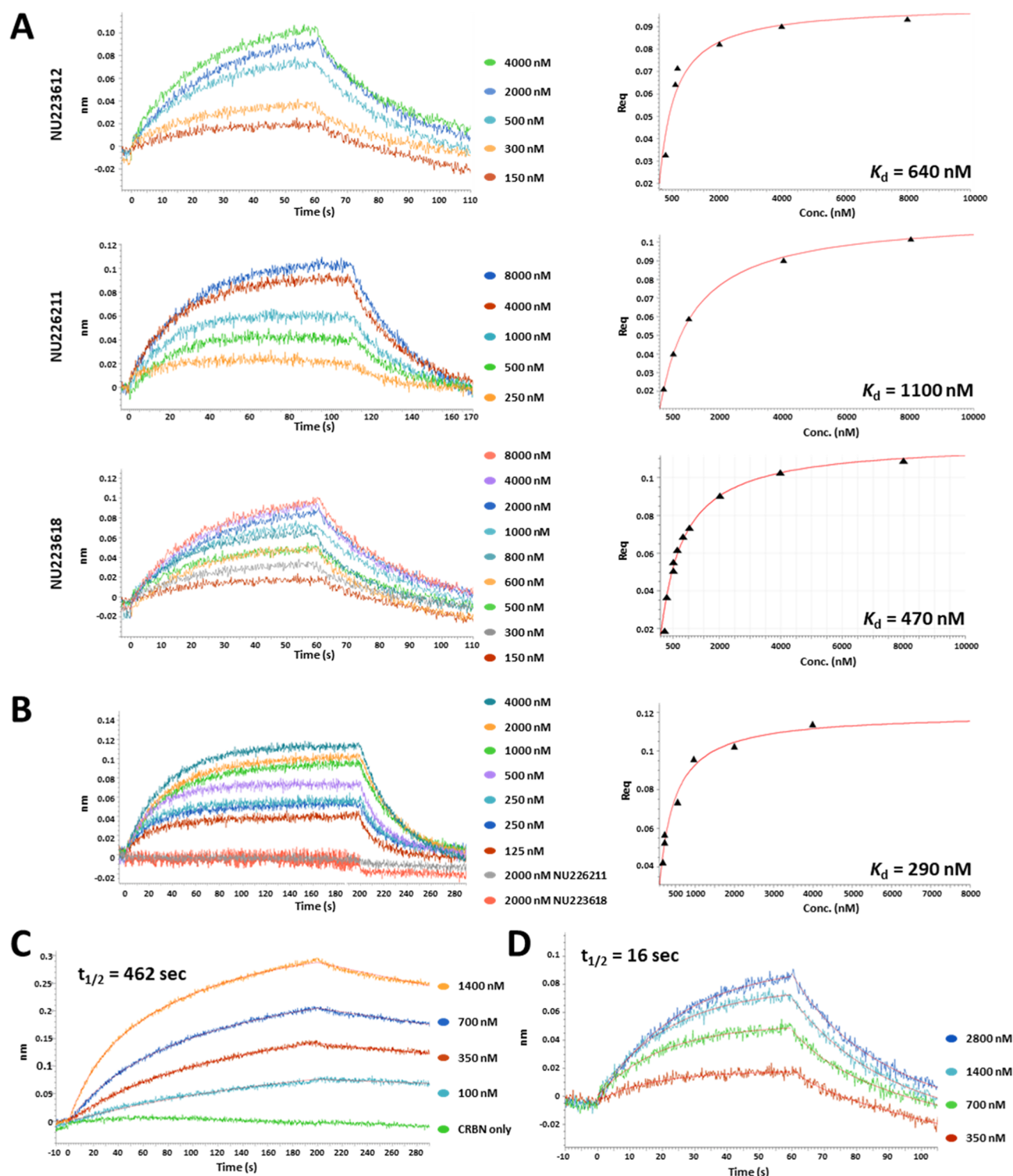


Figure 4. Mechanistic understanding of IDO1-PROTAC-induced IDO1 degradation. (A) Left: BLI sensorgrams showing the association and dissociation of compounds NU223612 (upper), NU226211 (middle), and NU223618 (lower) to the IDO1 protein pre-immobilized on NI NTA sensors. Right: For each complex, the equilibrium dissociation constant (K_d) was obtained by fitting the steady-state data (Req as a function of compound concentration) with a 1:1 binding model. (B) Left: Sensorgrams showing interactions of compounds with CRBN immobilized on AR2G sensors via amine coupling. Of the three compounds tested, only NU223612 shows measurable binding to CRBN. Right: Steady-state data plot and fit for the CRBN–NU223612 interaction. (C) BLI sensorgrams monitoring the association and dissociation kinetics of IDO1 binding of compound NU223612 pre-incubated with CRBN. Double-referenced data sets fitted globally with a 1:1 kinetic model yielded $k_{on} = 12,800$ M/s and $k_{off} = 0.0015$ sec⁻¹ for the ternary NU223612/CRBN/IDO1 complex. (D) BLI sensorgrams monitoring the association and dissociation kinetics of IDO1 binding of compound NU223612 to IDO1 alone. Double-referenced data sets fitted globally with a 1:1 kinetic model yielded $k_{on} = 68,900$ M/s $k_{off} = 0.042$ sec⁻¹ for the NU223612/IDO1 binary complex. No binding was detected between CRBN (25 mM) and IDO1 in the absence of NU223612 (trace “CRBN only” in C).

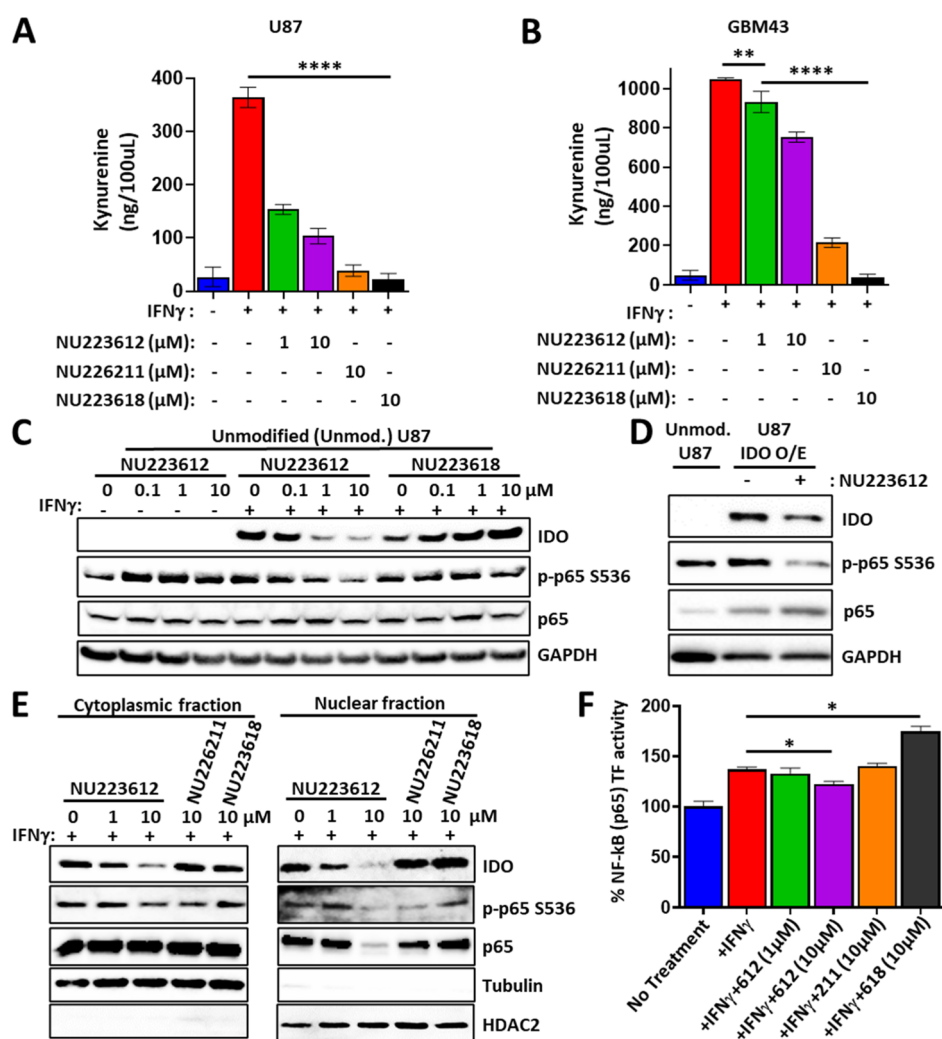


Figure 5. Effects of IDO1-PROTACs on IDO1 enzyme and non-enzyme-associated functions in GBM cells. (A,B) Effects of NU223612, NU226211, and NU223618 on kynurenine production in U87 and GBM43 human GBM cells. Cells were treated with NU223612, NU226211, or NU223618 in the presence of 50 ng/mL IFN γ for 24 h, and cell culture supernatants were collected to measure IFN γ -induced kynurenine levels using Ehrlich's reagent. Cells cultured in the absence of IFN γ served as the control group. (C) Western blotting analysis to determine the effect of NU223612 and NU223618 on IDO1 protein levels, phospho-p65 levels, total-p65 levels, and GAPDH levels in U87 cells. IDO1 protein was induced with IFN γ for 24 h in U87 cells, followed by treatment with NU223612 and NU223618 for 24 h at multiple concentrations. (D) Western blotting analysis to determine the effect of NU223612 on the levels of IDO1 protein, phospho-p65, total-p65 and GAPDH in U87 IDO1-FLAG cDNA-expressing cells. Cells were treated with DMSO or NU223612 (10 μ M) for 24 h prior to protein extraction. U87 parental cells served as a control group for basal phosphorylation of p65. (E) Western blotting analysis to determine the effect of NU223612 on cytoplasmic and nuclear levels of IDO1 protein, phospho-p65, total-p65, HDAC2 (nuclear marker), and tubulin (cytoplasmic marker) in U87 cells. Cells were treated with DMSO or NU223612 (10 μ M) for 24 h prior to protein extraction. (F) Graph representing NF- κ B-p65 specific transcription factor activity in nuclear extracts from U87 cells treated with NU223612, NU226211, or NU223618 (10 μ M). Relative optical density for each sample was corrected for total protein concentration, and NF- κ B p65 DNA binding activity is calculated as percent NF- κ B (p65) transcriptional factor activity relative to DNA binding activity observed in unstimulated U87 cells (data are mean \pm SEM). * P < 0.05, ** P < 0.01, **** P < 0.0001.

accordance with what others have previously suggested,²⁴ BLI may be more advantageous than surface plasmon resonance as a biophysical tool for characterization of ternary complexes in PROTAC studies. No interaction between the IDO1 and CRBN proteins was detected in the absence of NU223612.

In summary, our results indicate that NU223612 enhances ternary complex formation between the IDO1 and CRBN proteins. The measured affinity of the ternary complex was 117 nM, which confirms that the complex forms with positive cooperativity ($\alpha = K_d^{\text{binary}}/K_d^{\text{ternary}} = 2.5$). Additionally, the ternary complex has markedly enhanced stability ($t_{1/2} = 462$ s) as compared to $t_{1/2} = 16$ s for the binary complex. Several studies have linked positive cooperativity and enhanced stability of

PROTAC ternary complexes with an enhanced potency and efficiency of target degradation.^{37,38}

NU223612 Inhibits IDO1 Enzyme and Non-enzyme Functions. NU223612 dose-dependently inhibits IDO1 enzyme activity resulting in decreased Kyn levels in cultured IFN γ -stimulated GBM cells (Figure 5A,B). NU223612 also inhibits IDO1 enzyme activity in other cell types including human ovarian OVCAR5, prostate PC3, and pancreatic CD18 cancer cells (Figure S7A–C). Beyond the enzyme-dependent effects of IDO1, tumor cell IDO1 possesses non-canonical, non-enzyme-mediated functions that suppress the anti-cancer immune response and decrease survival.^{17,34,39} IDO1 non-enzyme activity was previously shown to involve the NF- κ B

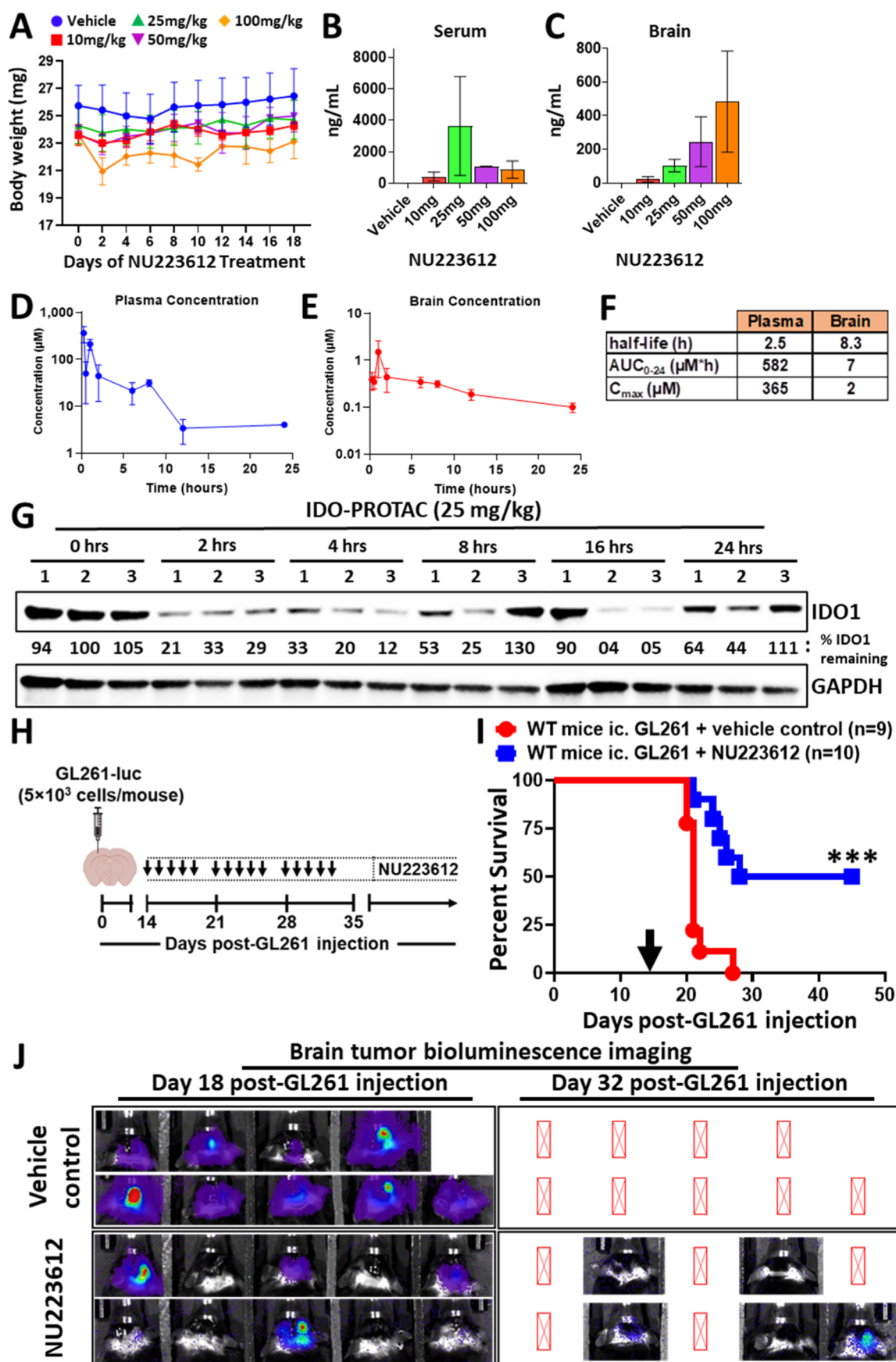


Figure 6. In vivo activity of the IDO1-PROTAC NU223612. (A) C57BL/6 male mice were treated with NU223612 ip. up to 3 weeks, once daily. Mouse body weight was measured every 2–3 days (mean \pm SEM; $n = 3$ mice/dose). (B) C57BL/6 mice were treated with NU223612 ip. for 3 weeks once daily. After 3 weeks of treatment, serum samples were prepared from the mice and subject to mass spectrometry analysis to quantify NU223612

Figure 6. continued

levels (mean \pm SEM; $n = 3$ mice/dose). (C) C57BL/6 mice were treated with NU223612 ip. for 3 weeks once per day. After 3 weeks of treatment, brain homogenate was prepared from the mice and subject to mass spectrometry analysis to quantify NU223612 levels (mean \pm SEM; $n = 3$ mice/dose). (D,E) PK of NU223612 in C57BL/6 mice. Mice were treated with NU223612 at 25 mg/kg ip. and serum and brain homogenate samples were collected for mass spectrometry analysis of NU223612 (mean \pm SEM; $n = 3$ mice/dose). (F) Half-life, AUC, and C_{\max} of NU223612 in serum and brain samples. (G) Western blotting analysis of IDO1 and GAPDH in tumor lysates. C57BL/6 were intracranially engrafted with mIDO1 cDNA-expressing GL261 cells. Three weeks after engraftment, mice were treated with NU223612 (25 mg/kg) and tumor samples were prepared at 0, 4, 8, 16, and 24 h for Western blotting analysis ($n = 3$ mice/time point). (H) Time line of 8 week old C57BL/6 wild-type (WT) mice that were intracranially engrafted with luciferase-modified GL261 cells (GL261-luc.) and treated with either vehicle (DMSO/EtOH/Tween80/HP-B-CD) control ($n = 9$ mice) or NU223612 (IDO1-PROTAC; $n = 10$ mice) loaded in the vehicle beginning 14 days after brain tumor cell injection. (I) Survival analysis of mice with brain tumors treated with either vehicle control or NU223612 as described in (H). Black arrow indicates the time point of treatment initiation. (J) Bioluminescence imaging of GL261 cell intracranial tumors at day 18 and day 32 post-GL261-luc. cell injection. *** $P < 0.001$.

(nuclear factor kappa B) pathway in murine dendritic cells.⁴⁰ Therefore, we investigated NU223612 for its potential to modulate NF- κ B signaling in human GBM cells. While NU223612 decreases p65 phosphorylation, neither NU226211 nor NU223618 inhibits NF- κ B phosphorylation in IFN γ -stimulated U87 GBM, GBM43, or MDA-MB-231 triple-negative breast cancer cells (Figures 5C; S8A,B). NU223612 also decreases p65 phosphorylation levels in the IDO1 cDNA-expressing human U87 GBM cell line and the mouse GL261 IDO1 cDNA-expressing murine cell line that is not treated with IFN γ (Figures 5D and S8C). To rule out potential non-specific effects of NU223612 on IDO1-dependent p65 phosphorylation, IDO1-PROTAC treatment was compared with IDO1 siRNA and IDO1 enzyme inhibitor treatment in U87 GBM and GBM43 cells. Although IDO1 siRNA and IDO1 enzyme inhibitor treatments both decrease Kyn levels (Figure S8D,E), only IDO1 siRNA treatment decreases NF- κ B p65 phosphorylation similar to the NU223612-mediated IDO1 protein degradation effects (Figure S8F,G). Interestingly, NU223612 decreases phosphorylated p65 levels in the nucleus of tumor cells (Figure 5E). In contrast, neither NU226211 nor NU223618 affects nuclear phosphorylated p65 protein levels. The net effect of NF- κ B nuclear translocation was determined by its DNA binding activity since p65 exerts its effect on gene expression by binding and transactivating the expression of target genes. To assess this, we performed a transcription factor ELISA assay on immobilized NF- κ B p65 response elements using nuclear extracts from U87 cells treated with NU223612, NU226211, or NU223618. Treatment with the IDO1-PROTAC significantly diminished transcription factor activity (Figure 5F) as a direct consequence of lower phosphorylated NF- κ B p65 levels in the nucleus (Figure S8H) as compared to cells treated with IFN γ alone (Figure 5G). Collectively, these data confirm that NU223612 inhibits both IDO1-mediated tryptophan metabolism as well as IDO1 non-enzyme-mediated NF- κ B p65 transcription factor DNA binding activity.

NU223612 Is Well Tolerated, Penetrates the Blood-Brain Barrier, Causes IDO1 Degradation in Brain Tumors, and Provides a Survival Advantage against Malignant Glioma. Male C57BL/6 mice were treated with NU223612 or NU223618, and compound levels were quantified in the serum and brain. Changes in body weight and overall survival were recorded. Vehicle and NU223612 were administered intraperitoneally (ip.) 5 days/week for 3 weeks at 10, 25, 50 mg/kg, or 100 mg/kg of body weight. The treatment of NU223612 did not result in significant body-weight changes at any dose during a three-week treatment time period (Figure 6A). However, the 100 mg/kg treatment of NU223612 was associated with

increased mortality (Figure S9A), and there is a precipitation of NU223612 observed around the intestines, liver, and pancreas of mice treated with both the 50 and 100 mg/kg doses. Mass spectrometry analysis of serum and brain tissue samples reveals the dose-dependent accumulation of NU223612 in serum and brain tissue, suggesting good bioavailability and BBB penetration of NU223612 in mice without brain tumors (Figure 6B,C). To establish PK parameters, C57BL/6 mice were ip. treated with a single 25 mg/kg dose of NU223612, followed by the quantification of drug concentrations in serum and brain at 0-, 0.25-, 0.5-, 1-, 2-, 6-, 8-, 12-, and 24 h time points. Mass spectrometry analysis of NU223612 (Figure 6D,E) shows a C_{\max} of 2 μ M and a half-life of 8.3 h in brain tissue (Figure 6F). In plasma, C_{\max} is 365 μ M and the half-life is 2.5 h. The binding of NU223612 to mouse brain homogenate using a 6 h equilibrium dialysis shows NU223612 to be 99.8% bound. Drug exposures were determined in other tissues as shown in Figure S9C–H. Pharmacodynamic (PD) analysis by western blot of intracranial tumors composed of GL261 cells expressing mIDO1 cDNA shows that a single ip. treatment with 25 mg/kg of NU223612 decreases IDO1 protein by >70% within 2 h post-treatment and remains low for up to 24 h (Figure 6G). The potential effect of NU223612 was next assessed on the overall survival of young 8 week old mice intracranially engrafted with GL261-luc. cells and treated with either vehicle alone or NU223612 beginning at 14 days post-GL261-luc. injection (Figure 6H). The treatment of mice with the IDO1-PROTAC led to an increase in median overall survival as well as longer-term survival for up to 45 days post-tumor cell injection (Figure 6I). The bioluminescence of intracranial tumor growth paralleled the survival data (Figure 6J). The data collectively suggest that the IDO1-PROTAC NU223612 has good bioavailability when administered ip., has sufficient brain exposure to degrade IDO1 protein in established intracranial brain tumors that express IDO1 and provides a survival benefit against malignant glioma when administered as a monotherapy.

DISCUSSION AND CONCLUSIONS

Although IDO1 is expressed at relatively negligible levels in a majority of tissues throughout the normal healthy body, it is significantly upregulated in a large number of human cancers, and in particular, those cancers that respond poorly to ICB-based immunotherapeutic approaches, including prostate cancer, pancreatic cancer, and GBM.⁴¹ In GBM, increased intratumoral IDO1 expression is associated with significantly decreased patient survival,¹² increased levels of intratumoral immunosuppressive regulatory T cells (Tregs, CD4⁺CD25⁺FoxP3⁺), and decreased survival of experimental animals with brain tumors.^{11,17} Although tumor cell IDO1

activity increases Tregs in glioma, and the treatment with a potent BBB-penetrating IDO1 enzyme inhibitor inhibits intratumoral kynurenine accumulation, the inhibition of tumor cell IDO1 enzyme activity fails to decrease intratumoral Treg accumulation and does not improve overall survival.^{17,31} The latter finding is in line with several reports showing that while IDO1 clearly possesses enzymatic functions, it also possesses non-canonical non-enzymic activities that non-redundantly suppress the anti-tumor immune response.^{17,34,40} The discovery that IDO1 possesses both enzyme- and non-enzyme-mediated effects, as well as clinical trial evidence showing that therapeutic IDO1 enzyme inhibition does not lead to improved cancer patient outcomes,^{10,42} motivated us to generate and characterize a compound that inhibits both IDO1 enzyme- and non-enzyme-mediated immunosuppressive functions.

The development of a targeted PROTAC allowed for IDO1 protein degradation, and in-turn, a viable strategy to simultaneously inhibit IDO1 enzyme- and non-enzyme-mediated functions in GBM cells. Recently, the design and synthesis of the first IDO1-PROTAC was reported.²⁹ This degrader was based on the IDO1 inhibitor epacadostat, a holo-IDO1 inhibitor, and displayed a $DC_{50} = 2.8 \mu M$ ²⁹ that is significantly weaker than the IDO1-PROTAC, NU223612, described here. There was also no in vivo evidence of IDO1-PROTAC effects combined with the known inability for epacadostat to enter the brain.⁴³ Herein, we report the development of an IDO1-PROTAC library utilizing the existing BMS-986205 (NU223618) apo-IDO1 inhibitor. The use of BMS-986205 allowed for the construction of a new IDO1-PROTAC class of molecules. Since this is the first report of the design and synthesis for apo-IDO1 inhibitor-derived PROTACs, we developed a diverse library to gain SAR data on the structural components required for IDO1 degradation. Ultimately the goal was to discover a molecule with BBB penetration and a desirable PK profile that would be suitable for the treatment of an intracranial brain tumor such as GBM. We constructed IDO1-PROTACs using a variety of CRBN- and VHL-directed E3 ligase ligands, an array of flexible and rigid linkers of differing lengths, and with multiple IDO1 ligand exit vectors. Screening U87 GBM cells that were stimulated to express IDO1 after treatment with human IFN γ enabled us to rapidly identify several active IDO1-PROTACs. NU223612 was discovered to be a moderately potent PROTAC that degrades IDO1 through a canonical ubiquitin-dependent proteasome-mediated mechanism.

Among the many recent studies that have been reported, there have been essentially no reports of PROTACs that achieve a brain exposure capable of producing a pharmacological effect, which may reflect their large size, flexible nature, large number of hydrogen bond donors, and/or a high polar surface area. Here we report a PROTAC that is capable of reaching pronounced levels in the brain. The lead compound, NU223612, reaches a concentration of 2 μM in brain tissue and is therapeutically effective. The results suggest that there is room for additional optimization of the lead compound that involves improving the potency and PK as well as improved parenchymal brain exposure of free drug. Importantly and as far as we know, this is the first work to demonstrate an IDO1-PROTAC that produces in vivo efficacy in a GBM model and therefore demonstrates a proof of concept for future translation into human patients with incurable GBM.

The therapeutic potential via targeting of IDO1 with an IDO1 enzyme inhibitor was recently challenged by the clinical

outcome of the phase 3, randomized, double-blind ECHO-301/KEYNOTE-252 trial.⁴² This trial found the combinatorial treatment of an IDO1 enzyme inhibitor with pembrolizumab (anti-PD-1 mAb) did not improve progression-free survival or overall survival of patients with unresectable or metastatic melanoma as compared to those patients who received a placebo plus pembrolizumab. There have been multiple suggestions to explain this result, including the possibility that the IDO1 enzyme inhibitor metabolically shunts tryptophan metabolism toward a compensatory serotonergic pathway.⁴⁴ Other possibilities include the involvement of the IDO1 paralog, IDO2, or TDO activities. Notably, there were no significant NU223612 effects on glioma cell IDO2 expression levels (Figure S10), and IDO2 does not readily metabolize tryptophan into kynurenine within physiological parameters.⁴⁵ TDO is a potent tryptophan metabolic enzyme expressed by GBM cells and liver hepatocytes.³³ There is yet another distinct possibility that is supported by ours as well as independent groups showing that IDO1 possesses both enzyme- and non-enzyme-mediated functions that collaborate and/or compensate for one another to suppress the immune response.^{17,40}

Aside from the effects mediated by IDO1 in cancer cells, it also plays an important immunosuppressive role in non-tumor cells. Specifically, IDO1 becomes therapeutically targetable with a pharmacologic IDO1 enzyme inhibitor in young mice with brain tumors after co-treatment with whole brain radiation (RT) and anti-PD-1 mAb.³¹ Importantly, while the IDO1 enzyme inhibitor is ineffective at improving overall survival in mice with brain tumors when administered as a monotherapy, the synergy of combining the IDO1 enzyme inhibitor with RT and anti-PD-1 mAb suggests that the latter treatment(s) causes IDO1 to be induced, upregulated, or functionally altered to ultimately render therapeutic targetability. This mechanism may be related to the enhanced IDO1-dependent tryptophan metabolism that occurs in brain tumor draining cervical lymph node cells.³⁹ Strikingly, however, the beneficial effects of pharmacologic IDO1 enzyme inhibitor treatment are ablated in older adult mice with brain tumors; hypothesized to be due to the increased extratumoral IDO1 expression in non-tumor cells of the aged brain that are refractory to IDO1 enzyme inhibition.^{20,34} Inhibiting all aspects of IDO1 activity with an IDO1-PROTAC may therefore be an effective future approach for controlling both enzyme- and non-enzyme-dependent processes in patients with aggressive ICB-resistant cancers.^{46,47} These data, coupled with our analysis of IDO1 in tumor cells, suggest that there are at least three populations of IDO1-expressing cells that can be considered when employing a maximally effective IDO1-targeting therapy: (i) tumor cell IDO1 that is refractory to IDO1 enzyme inhibition;^{10,11,31} (ii) non-tumor cell IDO1 in brain tumor draining cervical lymph node cells that is responsive to IDO1 enzyme inhibition;^{31,39} and (iii) extratumoral IDO1 expression by non-tumor cells in the older adult brain.^{34,48} Since different types of cells can express different E3 ubiquitin ligases, it is possible that multiple IDO1-PROTACs employing different E3 ligase ligands will be required to fully target all immunosuppressive IDO1-expressing cell types throughout the body.

This work is the first to develop an IDO1-PROTAC that is specifically designed for subjects with intracranial primary brain tumors. It's also the first time that this new tool has allowed for the dissection of IDO1 enzyme-versus non-enzyme-mediated effects in human cancer cells. Adult human GBM patients have a poor prognosis in part due to the anatomical location of the

tumor within the central nervous system that limits treatment options due to permeability restrictions of the blood-brain barrier. Future work will focus on optimizing the IDO1-PROTAC, **NU223612**, with an emphasis on the enhancement of IDO1 protein degradation potency and efficacy, retention time in the circulation, as well as improving brain exposure and PK. Since both enzymatic and non-enzymatic IDO1 effects contribute to its immunosuppressive properties, **NU223612** and future derivative compounds will be used to dissect the mechanistic contributions by both functions in GBM and possibly other types of IDO1-expressing cancers.

EXPERIMENTAL SECTION

General Chemical Methods. All chemical reagents were obtained from commercial suppliers and used without further purification, unless otherwise stated. Reactions were run without taking precautions to exclude air or moisture, unless otherwise noted. Normal-phase column chromatography was performed using silica gel columns and ACS grade solvents. Analytical thin-layer chromatography (TLC) was performed on EM Reagent 0.25 mm silica gel 60 F254 plates and visualized by UV light. ^1H NMR, ^{13}C NMR, and ^{19}F NMR spectroscopy were recorded on Bruker 400 MHz or Bruker Avance III 500 MHz spectrometers. The chemical shifts for ^1H NMR and ^{19}F NMR are reported to the second decimal place in parts per million (ppm). Proton coupling constants are expressed in hertz (Hz). Standard abbreviations were used to denote spin multiplicity for ^1H NMR data. The chemical shifts for ^{13}C NMR are reported to the first decimal place in ppm. The corresponding residual solvent peaks (CDCl_3 , ^1H δ = 7.27 ppm, ^{13}C δ = 77.16 ppm; $\text{CD}_3\text{OD}-d_4$, ^1H δ = 3.31 ppm, ^{13}C δ = 49.00 ppm; $\text{DMSO}-d_6$, ^1H δ = 2.50 ppm, ^{13}C δ = 39.52 ppm) were used as an internal standard. High-resolution mass spectrometry (HRMS) values were measured and calculated with an Agilent 6545 QTOF mass spectrometer coupled with an Agilent 1200 series LC, with direct loop injection (no column). All compounds presented in the manuscript are >95% pure by HPLC analysis.

(*R*)-*N*-(4-Chlorophenyl)-2-[(1*S*,4*S*)-4-(6-fluoroquinolin-4-yl)cyclohexyl]propanamide (**NU223618**, **2**). To a solution of previously described compound, **1**⁴⁹ (4.5 g, 14.9 mmol, 1.0 equiv) and 4-chloroaniline (2.3 g, 17.9 mmol, 1.2 equiv) in pyridine (90 mL) was added 3-(ethyliminomethylideneamino)propyl-dimethylazanium chloride (EDCI, 2.9 g, 14.9 mmol, 1.0 equiv) at 0 °C and the mixture was stirred at rt for 12 h, during which time the mixture maintained as a yellow solution. TLC [petroleum ether/tetrahydrofuran (THF), 1:1] showed that the starting material (R_f = 0.4) was consumed, and a new main spot (R_f = 0.2) was generated. The mixture was poured into a mixture of hydrochloric acid (HCl, 570 mL, 1N) and ethyl acetate (EtOAc, 800 mL). The two phases were separated, and the organic layer was washed with a saturated sodium carbonate (Na_2CO_3) solution (2 × 300 mL). The organic layer was then dried over anhydrous sodium sulfate (Na_2SO_4), filtered, and concentrated under reduced pressure to give **NU226318** (**2**) (5.3 g, 86%) as a yellow solid. ^1H NMR (500 MHz, $\text{CD}_3\text{OD}-d_4$): δ 8.77 (d, J = 4.7 Hz, 1H), 8.07 (dd, J = 9.3, 5.5 Hz, 1H), 7.89 (dq, J = 10.8, 2.3 Hz, 1H), 7.62–7.56 (m, 4H), 7.30 (d, J = 8.5 Hz, 2H), 3.47–3.38 (m, 1H), 2.88 (dq, J = 10.7, 6.8 Hz, 1H), 2.11–1.74 (m, 9H), 1.25 (d, J = 6.8 Hz, 3H) ppm. ^{13}C NMR (126 MHz, $\text{CD}_3\text{OD}-d_4$): δ 178.1, 163.1, 161.1, 155.4, 155.4, 150.5, 150.5, 146.1, 138.6, 132.8, 132.7, 130.1, 129.8, 129.3, 129.2, 122.7, 120.7, 120.5, 119.9, 108.3, 108.1, 42.5, 39.7, 37.5, 30.1, 29.2, 28.8, 27.8, 16.6 ppm. ^{19}F NMR (376 MHz, $\text{CD}_3\text{OD}-d_4$): δ –113.99 ppm. Spectra matched previously reported characterization data.¹ HRMS (m/z): [$M + \text{Na}$]⁺ calcd. For $\text{C}_{24}\text{H}_{24}\text{ClFN}_2\text{O}$ 433.1453; found, 433.1448. Purity 99.6% (HPLC).

tert-Butyl 4-(4-Nitrophenoxy)piperidine-1-carboxylate (**4**). To a solution of 1-fluoro-4-nitrobenzene **3** (15.8 g, 111.8 mmol, 1.5 equiv) and *tert*-butyl 4-hydroxypiperidine-1-carboxylate (15.0 g, 74.5 mmol, 1.0 equiv) in THF (400 mL) was added potassium *tert*-butoxide (16.7 g, 149.1 mmol, 2.0 equiv) portion-wise at 0 °C under nitrogen and the mixture was stirred at rt for 5 min, during which time the mixture

maintained as a brown solution. TLC (petroleum ether/EtOAc, 3:1) showed that the starting material (R_f = 0.1) was consumed, and a new main spot (R_f = 0.5) was generated. The mixture was poured into H_2O (50 mL) and concentrated under reduced pressure. The aqueous phase was extracted with EtOAc (3 × 40 mL). The organic phase was washed with brine (100 mL), dried over Na_2SO_4 , filtered, and concentrated under reduced pressure. The residue was purified by column chromatography (SiO_2 , petroleum ether/EtOAc, 100:1 to 3:2) to give **4** (23.0 g, 86%) as a brown solid. ^1H NMR (400 MHz, CD_3OD): δ 8.25–8.14 (m, 2H), 7.15–7.05 (m, 2H), 4.74 (tt, J = 7.5, 3.7 Hz, 1H), 3.80–3.68 (m, 2H), 3.36 (br t, J = 9.1 Hz, 2H), 2.04–1.95 (m, 2H), 1.77–1.62 (m, 2H), 1.47 (s, 9H) ppm. Spectral data matched previously reported characterization data.⁵⁰

tert-Butyl 4-(4-Aminophenoxy)piperidine-1-carboxylate (**5**). To a solution of **4** (17.0 g, 52.7 mmol, 1.0 equiv) in methanol (MeOH, 340 mL) was added Pd/C (2.8 g, 10% Pd on charcoal, wet, containing 50% H_2O) at rt. The mixture was stirred at rt for 6 h in a H_2 atmosphere (15 Psi). TLC (petroleum ether/EtOAc, 1:1) showed the starting material (R_f = 0.9) was consumed, and a new main spot (R_f = 0.4) was generated. The reaction mixture was filtered. The filtrate was concentrated to give **5** (15.0 g, 88%) as a brown solid, which was used for the next step without further purification. ^1H NMR (400 MHz, CD_3OD): δ 6.82–6.75 (m, 2H), 6.74–6.66 (m, 2H), 4.35 (tt, J = 7.4, 3.6 Hz, 1H), 3.76–3.66 (m, 2H), 3.35–3.24 (m, 3H), 1.93–1.84 (m, 2H), 1.67–1.58 (m, 2H), 1.51–1.46 (m, 9H) ppm. Spectral data matched previously reported characterization data.⁵⁰

(*R*)-2-[(1*S*,4*S*)-4-(6-Fluoroquinolin-4-yl)cyclohexyl]-*N*-[4-(piperidin-4-yloxy)phenyl]propanamide (**6**). To a solution of **1** (2.5 g, 8.3 mmol, 1.0 equiv) and **5** (2.8 g, 9.5 mmol, 1.1 equiv) in pyridine (25 mL) was added EDCI (2.4 g, 12.4 mmol, 1.5 equiv) at 0 °C, and the mixture was stirred at rt for 12 h, during which time the mixture maintained as a yellow solution. TLC (petroleum ether/THF, 1:1) showed that the starting material (R_f = 0.4) was consumed, and a new main spot (R_f = 0.2) was generated. Additional three reactions were set up, as described above, and combined for purification. The combined reaction mixture was poured into 1 N HCl (120 mL) and EtOAc (200 mL). The two phases were separated, and the aqueous phase was extracted with EtOAc (2 × 50 mL). The combined organic layers were washed with 1 N HCl (2 × 30 mL), saturated Na_2CO_3 solution (3 × 100 mL), then dried over anhydrous Na_2SO_4 , filtered, and concentrated under reduced pressure to give a boc-protected intermediate (19.0 g, 95% yield) as a yellow solid, which was taken forward without further purification. To a solution of boc-protected intermediate (6.0 g, 10.4 mmol, 1.0 equiv) in dioxane (10 mL) was added HCl/dioxane (4 M, 40 mL) at rt. The reaction mixture was stirred at rt for 12 h. TLC (petroleum ether/THF, 1:1) showed that the starting material (R_f = 0.2) was consumed, and a new main spot (R_f = 0.01) was generated. Additional two reactions were set up, as described above, and combined for purification. The combined reaction mixtures were concentrated under reduced pressure to give **6** (16.0 g, HCl salt, 97%) as a yellow solid. ^1H NMR (500 MHz, $\text{DMSO}-d_6$): δ 10.27 (s, 1H), 9.31 (d, J = 28.1 Hz, 2H), 8.88 (d, J = 4.7 Hz, 1H), 8.13 (dd, J = 9.2, 5.7 Hz, 1H), 8.02 (dd, J = 10.9, 2.8 Hz, 1H), 7.78 (d, J = 4.7 Hz, 1H), 7.74–7.66 (m, 1H), 7.64–7.57 (m, 2H), 6.98–6.88 (m, 2H), 4.56 (tt, J = 7.3, 3.3 Hz, 1H), 3.40 (td, J = 11.1, 5.6 Hz, 2H), 3.120–3.16 (m, 2H), 3.05–2.97 (m, 3H), 2.15–1.51 (m, 13H), 1.09 (d, J = 6.6 Hz, 3H) ppm. ^{13}C NMR (126 MHz, $\text{DMSO}-d_6$): δ 174.6, 161.1, 159.2, 154.1, 152.1, 149.1, 144.0, 133.3, 131.8, 131.7, 127.4, 120.8, 119.8, 119.6, 119.3, 116.2, 107.6, 107.4, 69.7, 48.6, 40.3, 37.9, 35.7, 28.6, 27.9, 27.3, 27.1, 26.5, 16.3 ppm. ^{19}F NMR (470 MHz, $\text{DMSO}-d_6$): δ –112.39 ppm. HRMS (m/z): [$M + \text{H}$]⁺ calcd. for $\text{C}_{29}\text{H}_{35}\text{FN}_3\text{O}_2$ 476.2724; found, 476.2708. Purity 99.6% (HPLC).

tert-Butyl 3-(2-(2-((2-(2,6-Dioxopiperidin-3-yl)-1,3-dioxoisindolin-4-yl)amino)ethoxy)ethoxy)propanoate (**9**). To a solution of 2-(2,6-dioxopiperidin-3-yl)-4-fluoroisindoline-1,3-dione **7** (25.6 g, 92.6 mmol, 1.2 equiv) and *tert*-butyl 3-(2-(2-aminoethoxy)ethoxy)propanoate (18.0 g, 77.2 mmol, 1.0 equiv) in dimethylformamide (DMF, 180 mL) was added *N,N*-diisopropylethylamine (DIPEA, 10.0 g, 77.2 mmol, 1.0 equiv) at rt. The mixture was stirred at 80 °C for 12 h, during which time the mixture was maintained as a green solution. TLC (petroleum ether/EtOAc, 1:2) showed that the starting material (R_f =

0.1) was consumed, and a new main spot ($R_f = 0.4$) was generated. The mixture was diluted with water (H_2O , 100 mL) and extracted with EtOAc (3×100 mL). The combined organic layers were washed with brine (200 mL), dried over Na_2SO_4 , filtered, and concentrated under reduced pressure to give a crude product. The residue was purified by column chromatography (SiO_2 , petroleum ether/EtOAc, 100:1 to 2:3) to give **9** (5.7 g, 14%) as a green solid. 1H NMR (400 MHz, $CDCl_3$): δ 8.15 (br s, 1H), 7.50 (dd, $J = 8.4, 7.2$ Hz, 1H), 7.11 (d, $J = 7.1$ Hz, 1H), 6.93 (d, $J = 8.5$ Hz, 1H), 6.50 (br s, 1H), 4.92 (dd, $J = 12.1, 5.3$ Hz, 1H), 4.13 (q, $J = 7.1$ Hz, 1H), 3.75–3.70 (m, 4H), 3.68–3.62 (m, 4H), 3.47 (t, $J = 5.4$ Hz, 2H), 2.89–2.67 (m, 3H), 2.52 (t, $J = 6.6$ Hz, 2H), 2.16–2.09 (m, 1H), 1.45 (s, 9H) ppm. Spectral data matched previously reported characterization data.⁵¹

3-(2-(2-((2-(2,6-Dioxopiperidin-3-yl)-1,3-dioxoisindolin-4-yl)-amino)ethoxy)ethoxy)propanoic Acid (11). A solution of **9** (3.6 g, 7.4 mmol) in HCl/dioxane (4 M, 36 mL) was stirred at rt for 6 h, during which time the mixture maintained as a green solution. TLC (petroleum ether/EtOAc 1:2) showed that the starting material ($R_f = 0.4$) was consumed, and a new main spot ($R_f = 0.1$) was generated. The mixture was concentrated under reduced pressure to give **11** (3.2 g, HCl salt, 83%) as a green solid. 1H NMR (400 MHz, $CDCl_3$): δ 8.77 (s, 1H), 7.53–7.44 (m, 1H), 7.09 (d, $J = 7.0$ Hz, 1H), 6.91 (d, $J = 8.5$ Hz, 1H), 4.98–4.89 (m, 1H), 3.77 (t, $J = 6.3$ Hz, 2H), 3.74–3.71 (m, 2H), 3.66 (s, 4H), 3.46 (br t, $J = 5.2$ Hz, 2H), 2.91–2.70 (m, 3H), 2.64 (t, $J = 6.3$ Hz, 2H) 2.16–2.08 (m, 1H) ppm. Spectral data matched previously reported characterization data.⁵¹

(2R)-N-(4-((1-(3-(2-(2-((2-(2,6-Dioxopiperidin-3-yl)-1,3-dioxoisindolin-4-yl)amino)ethoxy)ethoxy)propanoyl)piperidin-4-yl)oxy)phenyl)-2-((1S,4S)-4-(6-fluoroquinolin-4-yl)cyclohexyl)propanamide (NU223612, 13). To a solution of **11** (7.0 g, 16.2 mmol, 1.0 equiv) in DMF (85 mL) was added HATU (7.4 g, 19.5 mmol, 1.2 equiv) and DIPEA (6.3 g, 48.6 mmol, 8.5 mL, 3.0 equiv) at 0 °C. The reaction mixture was stirred for 30 min. After that, **6** (8.3 g, 16.21 mmol, 1.0 equiv) was added to the reaction, and the mixture was stirred at rt for 12 h. TLC (EtOAc/MeOH, 5:1) showed that the starting material ($R_f = 0.02$) was consumed, and a new main spot ($R_f = 0.2$) was generated. The reaction mixture was poured into H_2O (150 mL) and extracted with EtOAc (300 mL). The organic layer was washed with brine (2×100 mL), dried over Na_2SO_4 , filtered, and concentrated under reduced pressure. The residue was purified by flash chromatography over silica gel (EtOAc-THF gradient from 0 to 100%). Pure fractions were combined, concentrated, and dried under high vacuum to give a residue, and then the residue was purified by recrystallization from dichloromethane (DCM)/EtOAc/petroleum ether (30 mL, 1:1:1) to give **NU223612 (13)** (6.4 g, 42%) as a yellow solid. 1H NMR (500 MHz, $DMSO-d_6$): δ 11.10 (s, 1H), 9.85 (s, 1H), 8.86 (d, $J = 4.5$ Hz, 1H), 8.09 (dd, $J = 9.2, 5.8$ Hz, 1H), 7.98 (dd, $J = 11.0, 2.8$ Hz, 1H), 7.67 (td, $J = 8.7, 2.8$ Hz, 1H), 7.61–7.43 (m, 4H), 7.13 (d, $J = 8.6$ Hz, 1H), 7.03 (d, $J = 7.0$ Hz, 1H), 6.95–6.86 (m, 2H), 6.60 (t, $J = 5.8$ Hz, 1H), 5.05 (dd, $J = 12.7, 5.4$ Hz, 1H), 4.49 (dt, $J = 7.9, 4.0$ Hz, 1H), 3.84–3.77 (m, 1H), 3.73–3.40 (m, 13H), 3.23–3.13 (m, 1H), 2.94–2.75 (m, 2H), 2.60–2.41 (m, 3H), 2.10–1.35 (m, 16H), 1.11 (d, $J = 6.6$ Hz, 3H) ppm. ^{13}C NMR (126 MHz, $DMSO-d_6$): δ 174.4, 172.9, 170.2, 169.0, 168.8, 167.4, 161.0, 159.0, 152.7, 152.6, 149.8, 146.5, 145.2, 136.3, 132.7, 132.1, 127.3, 120.9, 119.2, 119.0, 118.8, 117.5, 116.3, 110.7, 109.3, 107.4, 107.2, 72.1, 69.8, 68.9, 67.0, 48.6, 42.2, 41.7, 38.2, 37.6, 35.7, 32.8, 31.0, 31.0, 30.3, 28.6, 27.8, 27.4, 26.5, 22.2, 16.3 ppm. ^{19}F NMR (376 MHz, $DMSO-d_6$): δ -112.94 ppm. HRMS (m/z): $[M + H]^+$ calcd. for $C_{49}H_{56}FN_3O_8$ 891.4087; found, 891.4063. Purity 96.5% (HPLC).

4-Fluoro-2-(1-methyl-2,6-dioxopiperidin-3-yl)isoindoline-1,3-dione (8). To a solution of **7** (4.2 g, 15.1 mmol, 1.0 equiv) in DMF (40 mL) was added MeI (12.9 g, 90.6 mmol, 6.0 equiv) and potassium carbonate (K_2CO_3 , 3.1 g, 22.6 mmol, 1.5 equiv) at 0 °C. The reaction mixture was stirred at rt for 12 h, during which time the mixture maintained as a yellow solution. TLC (petroleum ether/EtOAc, 1:1) showed that the starting material ($R_f = 0.3$) was consumed, and a new main spot ($R_f = 0.4$) was generated. The mixture was diluted with H_2O (100 mL) and extracted with EtOAc (3×100 mL). The combined organic layers were washed with brine (200 mL) and dried over

Na_2SO_4 , filtered, and concentrated under reduced pressure to give **8** (3.6 g, 73%) as a white solid, which was used in the next step without further purification. 1H NMR (400 MHz, $CDCl_3$): δ 7.81–7.74 (m, 1H), 7.74–7.69 (m, 1H), 7.43 (t, $J = 8.4$ Hz, 1H), 5.08–4.93 (m, 1H), 3.22 (s, 3H), 3.05–2.95 (m, 1H), 2.86–2.73 (m, 2H), 2.17–2.10 (m, 1H) ppm. Spectral data matched previously reported characterization data.⁵¹

tert-Butyl 3-(2-(2-((2-(1-methyl-2,6-dioxopiperidin-3-yl)-1,3-dioxoisindolin-4-yl)amino)ethoxy)ethoxy)propanoate (10). To a solution of *tert*-butyl 3-(2-(2-aminoethoxy)ethoxy)propanoate (3.4 g, 14.7 mmol, 1.2 equiv) in DMF (20 mL) was added DIPEA (1.6 g, 12.3 mmol, 1.0 equiv) and **8** (3.6 g, 12.3 mmol, 1.0 equiv) at rt and the mixture was stirred at rt for 12 h, during which time the mixture maintained as a green solution. TLC (petroleum ether/EtOAc, 1:1) showed that the starting material ($R_f = 0.4$) was consumed, and a new main spot ($R_f = 0.3$) was generated. The mixture was diluted with H_2O (100 mL) and extracted with EtOAc (3×100 mL). The combined organic layers were washed with brine (200 mL) and dried over Na_2SO_4 , filtered, and concentrated under reduced pressure to give a crude product. The residue was purified by column chromatography (SiO_2 , petroleum ether/EtOAc, 100:1 to 3:2) to give **10** (1.8 g, 26%) as a green solid. 1H NMR (400 MHz, $CDCl_3$): δ 7.50 (dd, $J = 8.4, 7.3$ Hz, 1H), 7.11 (d, $J = 6.9$ Hz, 1H), 6.93 (d, $J = 8.5$ Hz, 1H), 6.49 (br s, 1H), 6.53–6.44 (m, 1H), 4.96–4.88 (m, 1H), 3.77–3.68 (m, 4H), 3.68–3.60 (m, 4H), 3.52–3.43 (m, 2H), 3.22 (s, 3H), 3.04–2.92 (m, 1H), 2.84–2.70 (m, 2H), 2.51 (t, $J = 6.6$ Hz, 2H), 2.16–2.06 (m, 1H), 1.46–1.43 (m, 9H) ppm. ^{13}C NMR (126 MHz, $CDCl_3$): δ 171.4, 171.1, 169.6, 169.1, 167.9, 146.9, 136.1, 132.6, 116.9, 111.7, 110.5, 80.7, 70.7, 70.5, 69.7, 67.1, 49.7, 42.5, 36.4, 32.1, 28.2, 27.4, 22.2 ppm. HRMS (m/z): $[M + Na]^+$ calcd. for $C_{25}H_{33}N_3O_8Na$ 526.2160; found, 526.2157.

3-(2-(2-((2-(1-Methyl-2,6-dioxopiperidin-3-yl)-1,3-dioxoisindolin-4-yl)amino)ethoxy)ethoxy)propanoic Acid (12). To a solution of **10** (1.8 g, 3.6 mmol, 1.0 equiv) was added HCl/dioxane (4 M, 18 mL) at rt, and the mixture was stirred at 20 °C for 6 h, during which time the mixture was maintained as a green solution. TLC (petroleum ether/EtOAc, 1:1) showed that the starting material ($R_f = 0.4$) was consumed, and a new main spot ($R_f = 0.1$) was generated. The mixture was concentrated under reduced pressure to give **12** (1.6 g, 83% yield) as a green solid and taken forward without further purification. 1H NMR (400 MHz, $CDCl_3$): δ 7.54–7.46 (m, 1H), 7.11 (d, $J = 7.1$ Hz, 1H), 6.93 (d, $J = 8.5$ Hz, 1H), 4.97–4.88 (m, 1H), 3.78 (t, $J = 6.2$ Hz, 2H), 3.74–3.71 (m, 3H), 3.67 (s, 4H), 3.48 (t, $J = 5.3$ Hz, 2H), 3.22 (s, 3H), 3.03–2.93 (m, 1H), 2.82–2.73 (m, 2H), 2.64 (t, $J = 6.2$ Hz, 2H), 2.14–2.05 (m, 1H) ppm.

(2R)-2-((1S,4S)-4-(6-Fluoroquinolin-4-yl)cyclohexyl)-N-(4-((1-(3-(2-(2-((2-(1-methyl-2,6-dioxopiperidin-3-yl)-1,3-dioxoisindolin-4-yl)amino)ethoxy)ethoxy)propanoyl)piperidin-4-yl)oxy)phenyl)propanamide (NU226211, 14). To a solution of **12** (1.5 g, 3.4 mmol, 1.0 equiv) in DMF (20 mL) was added HATU (1.5 g, 4.0 mmol, 1.2 equiv) and DIPEA (2.2 g, 16.8 mmol, 5.0 equiv) at 0 °C. The reaction mixture was stirred for 30 min. After that, **6** (1.6 g, 3.4 mmol, 1.0 equiv) was added to the reaction, and the mixture was stirred at 20 °C for 12 h. TLC (EtOAc/MeOH, 5:1) showed that the starting material ($R_f = 0.02$) was consumed, and a new main spot ($R_f = 0.2$) was generated. The reaction mixture was poured into H_2O (50 mL) and extracted with EtOAc (150 mL). The organic layer was washed with brine (2×50 mL), dried over Na_2SO_4 , filtered, and concentrated under reduced pressure. The residue was purified by flash chromatography over silica gel (EtOAc-THF gradient from 0 to 100%). Pure fractions were combined, concentrated, and dried under high vacuum to give **NU226211 (14)** (1.5 g, 48%) as a light green solid. 1H NMR (500 MHz, $DMSO-d_6$): δ 9.85 (s, 1H), 8.86 (d, $J = 4.5$ Hz, 1H), 8.09 (dd, $J = 9.2, 5.8$ Hz, 1H), 7.98 (dd, $J = 11.0, 2.8$ Hz, 1H), 7.67 (td, $J = 8.7, 2.8$ Hz, 1H), 7.61–7.47 (m, 4H), 7.14 (d, $J = 8.6$ Hz, 1H), 7.03 (d, $J = 7.0$ Hz, 1H), 6.90 (d, $J = 8.8$ Hz, 2H), 6.61 (t, $J = 5.8$ Hz, 1H), 5.11 (dd, $J = 13.0, 5.4$ Hz, 1H), 4.49 (br s, 1H), 3.84–3.76 (m, 1H), 3.65–3.45 (m, 13H), 3.23–3.17 (m, 1H), 3.00 (s, 3H), 2.97–2.72 (m, 4H), 2.08–1.39 (m, 16H), 1.11 (d, $J = 6.6$ Hz, 3H) ppm. ^{13}C NMR (126 MHz, $DMSO-d_6$): δ 174.4, 171.9, 169.9, 169.0, 168.7, 167.3, 161.0, 159.0, 152.6, 152.6, 149.8, 146.5, 145.2, 136.3, 132.7, 132.1, 127.3, 120.8, 119.2,

119.0, 118.8, 117.6, 116.2, 110.7, 109.2, 107.4, 107.2, 72.1, 69.7, 68.9, 67.0, 49.2, 42.2, 41.7, 38.2, 37.6, 35.7, 32.8, 31.2, 31.0, 30.3, 28.6, 27.8, 27.4, 26.7, 26.4, 21.4, 16.3 ppm. ^{19}F NMR (376 MHz, DMSO- d_6): δ -112.96 ppm. HRMS (m/z): $[\text{M} + \text{H}]^+$ calcd. for $\text{C}_{50}\text{H}_{58}\text{FN}_6\text{O}_9$ 905.4244; found, 905.4221. Purity 98.0% (HPLC).

Mice and Cell Lines. 8 week old male wild-type C57BL/6 (Cat#000664) mice were obtained from Jackson Laboratories and maintained in the Northwestern University Center for Comparative Medicine (CCM). All of the procedures involving animals were conducted in accordance with the Institutional Animal Care and Use Committee (IACUC) of Northwestern University. The human U87 GBM cell line, GBM43 and GBM6 patient-derived xenografts (PDXs) from human adults, the DIPG007 high-grade glioma cell line from a human child, and the GL261 glioma cell line from a C57BL/6 mouse were obtained from the American Type Culture Collection (ATCC), Drs. C. David James, Ph.D., or Rintaro Hashizume, M.D./Ph.D. Human pancreatic, ovarian, breast, and prostate cancer cell lines were provided by Drs. Hidayatullah Munshi, M.D., Daniela Matei, M.D., Marcelo Bonini, Ph.D., and Jennifer D. Wu, Ph.D., respectively. A comprehensive list of human cancer cells used with their respective culture conditions is shown in Table S1. Cells were cultured at 37 °C in a humidified chamber containing 5% CO_2 as described.⁵²

siRNA Transfection and Western Blotting. A short interfering RNA (siRNA) duplex targeting human IDO1 was synthesized by Dharmacon. For transfection in GBM cells, either ON-TARGET plus control siRNA (scrambled siRNA: siSCR) or IDO1-targeting ON-TARGET plus siRNA-SMART pool (siIDO1) were transfected using Lipofectamine 3000 transfection reagent (ThermoFisher, Cat# L3000001) according to the manufacturer's protocol. Protein samples were prepared by lysing the cells in RIPA buffer (Sigma-Aldrich, Cat# R0278) supplemented with protease and phosphatase inhibitors on ice for 30 min. Cell lysates were clarified by centrifugation at 16,000g for 15 min at 4 °C. Equal amounts of proteins, as quantified by bicinchoninic acid assay (Pierce), were separated on an SDS-polyacrylamide gel electrophoresis, and proteins were electrophoretically transferred onto a polyvinylidene fluoride (PVDF) membrane using a Trans-Blot Turbo Transfer System (Bio-Rad, Hercules, CA, USA). The blotted membranes were blocked for 1 h at room temperature in blocking buffer containing 5% (w/v) nonfat dry milk in Trisbuffered saline and 0.1% Tween 20 (TBS-T), followed by incubating the membranes overnight at 4 °C with primary antibodies against a target protein diluted at a standardized concentration in blocking buffer. The blots were washed three times with TBS-T and incubated for 1 h at room temperature with horseradish peroxidase-conjugated secondary antibody generated against the host antigen in which the primary antibody was generated. The protein bands were detected using an enhanced chemiluminescence reagent (SuperSignal West Femto Maximum Sensitivity substrate), and blots were visualized with Bio-Rad ImageLab software on a Bio-Rad ChemID01c MP imaging system. All blots were stripped and re-probed with glyceraldehyde phosphate dehydrogenase (GAPDH) to ensure the proteins were loaded equally across all the samples in a particular blot. Western blotting analysis for proteins of interest used antibodies at optimized concentrations. The full list of antibodies utilized throughout this study is provided in Table S2.

Isolation of Nuclear and Cytoplasmic Fractions. The nuclear and cytoplasmic fractions that were isolated from GBM cells were prepared using an NE-PER Nuclear and Cytoplasmic Extraction Reagent kit (ThermoFisher, Cat#788835) as per the manufacturer's protocol. Isolated nuclear and cytoplasmic fractions underwent western blot analysis as described above and were assayed for expression of IDO1, phospho-p65, and total-p65. Expression of HDAC2 and β -tubulin were used as nuclear and cytoplasmic markers, respectively.

Ubiquitination Assay. 500 μg of cell lysate from stably expressing U87 flag-tagged human IDO1 cDNA was added to Eppendorf tubes containing 30 μL of protein A/G beads (Santa Cruz, Cat# sc-2003) and 1 μg of M2-Flag antibody (Sigma-Aldrich, Cat# F-1804). The complex was incubated at 4 °C overnight on a shaker, followed by bead washing with 500 μL of RIPA buffer three times. Immunoprecipitated proteins were eluted directly into 2 \times lamellae sample buffer with β -mercaptoethanol and boiled for 5 min. Samples underwent western

blot analysis, and membranes were probed with anti-IDO1 (1:8000) and anti-ubiquitin (1:3000) mAbs.

NF- κB (RelA/p65) Transcription Factor ELISA Assay. To determine the NF- κB p65 levels in nuclear and cytoplasmic fractions after IDO1-PROTAC treatment, an NF- κB transcription factor assay kit was used (Abnova) to detect NF- κB (p65) specific DNA binding activity in nuclear extracts. The nuclear and cytoplasmic extracts from unstimulated U87 cells or interferon gamma ($\text{IFN}\gamma$)-stimulated U87 cells treated with either DMSO, IDO1-PROTAC (NU223612), inactive IDO1-PROTAC (NU226211), or IDO1 enzyme inhibitor (NU223618) were prepared using a protocol mentioned in a previous version of this kit (NF- κB - p65, Transcription Factor Assay Kit Version: 06), followed by assaying the nuclear extracts as per the manufacturer's instructions provided in the kit (Transcription Factor Assay Kit Version: 11).

Kynurenine Assay. Kynurenine levels in cell culture supernatants were measured using Ehrlich's reagent.⁵³ Briefly, cell culture supernatants were incubated with a 10% final concentration of trichloroacetic acid in Eppendorf tubes for 20 min at 60 °C to release kynurenine from cells and to precipitate proteins. After 20 min, samples were centrifuged for 20 min at 2500g, and supernatants were mixed with 20 mg/mL 4-dimethylamino benzaldehyde in acetic acid (Sigma-Aldrich) at a 1:1 ratio, and absorbance was measured at 480 nm using a plate reader.

BLI Assays. A FortéBio Octet K2 BLI instrument (Sartorius) was used for studying the interactions of NU223612 (IDO1-PROTAC), NU226211 (inactive IDO1-PROTAC), and NU223618 (IDO1 enzyme inhibitor) with the IDO1 and cereblon (CRBN) proteins. 6xHis-tagged recombinant IDO1 protein (purchased from Active Motif, Carlsbad, CA, Cat# 81031) was reconstituted at 80 $\mu\text{g}/\text{mL}$ and treated with human apo-myoglobin (Prospec Cat#PRO-374) in order to remove residual heme groups. This procedure, adapted from Nelp and co-workers,²⁶ consisted of incubating IDO1 with 5-fold excess apo-myoglobin for 1 h at 37 °C. The IDO1 protein was then loaded on pre-hydrated Ni-NTA biosensors (Sartorius, FortéBio, Cat# 18-5103). The concentration of IDO1 in the loading step was 55 $\mu\text{g}/\text{mL}$, and the duration of the loading step was 360 s. The BLI signal stabilized at a value of 6 nm after approximately 220 s. No dissociation of the IDO1 protein was observed for 30 min when the sensors were moved into buffer (PBS + 0.5% DMSO at pH 7.4). at 30 °C.

For studies of the binary complexes between NU223612, NU223618, or NU226211 with IDO1, compounds were diluted in reaction buffer to obtain a stock concentration of 80 μM . After baseline equilibration in the reaction buffer, the kinetics of association were monitored by moving individual sensors into wells containing 200 μL of analyte solution for each complex. After the association step, the sensors were placed in the reaction buffer to monitor dissociation. During the entirety of the kinetic assay, the 96-well sample plate was kept at 30 °C and was shaken at 1,000 rpm. Biosensors without ligands were titrated with an analyte and used as a parallel reference control. Ligand-loaded biosensors without analytes were used as a baseline. Double-referenced data were fitted globally with a steady-state 1:1 model using the Data Analysis HT 11.0.0.50 (FortéBio) software suite.

For examining the interaction of CRBN with NU223612, NU223618, and NU226211, BLI experiments and data analysis were performed as described above, except sensors with immobilized CRBN were used instead. To prepare the sensors, CRBN protein (Sino Biological, Wayne, PA) was reconstituted in an acetate buffer at pH 6 and amine coupled to AR2G sensors (Sartorius, FortéBio, Cat# 18-5092) following the manufacturer's recommendations. For experiments examining the formation of a ternary complex, IDO1 was immobilized on NiNTA sensors as described above from 20 $\mu\text{g}/\text{mL}$ solutions. To form the NU223612-CRBN complex, NU223612 at 1.4 μM was pre-incubated with a 25 molar excess of CRBN⁴⁰ and allowed to equilibrate for 15 min at 30 °C. A series of 2-fold dilutions of this stock solution were made; these dilutions were allowed to equilibrate for an additional 15 min at 30 °C before binding reactions between IDO1 and the NU223612-CRBN complex were monitored. Separately, experiments with identical sequences and preparation were performed using NU223612 without CRBN and with CRBN without NU223612. For ternary and binary complexes, each dataset was globally fitted with a 1:1

kinetic model using the Data Analysis HT 11.0.0.50 (FortéBio) software.

Isothermal Titration Calorimetry. ITC experiments were performed using a MicroCal ITC₂₀₀ instrument (Malvern Panalytical). The CRBN protein was dialyzed in PBS + 0.5% DMSO, pH 7.4, and diluted to a final concentration of 6 μ M. After filtration through 0.22 μ m Millipore centrifugal units, the concentration of the protein solution was checked using a NanoDrop spectrophotometer. Solutions were then degassed for 5 min and loaded into the ITC sample cell. An equal volume (280 μ L) of filtered Millipore water was placed in the reference cell. Each test compound was diluted from a 30 mM DMSO stock to a final concentration of 120 μ M in PBS + 0.5% DMSO, pH 7.4. After degassing for 10 min, 40 μ L of the compound solution was loaded into the injection syringe. The ITC instrument was equilibrated at 30 °C and 1,000 rpm syringe rotational speed. The first injection of 0.1 μ L was performed followed by 15 injections of 1.5 μ L volume spaced at 100 s. ITC data were processed with the MicroCal Origin 7.0 software package as described.⁵⁴ Individual injection heats (qi)—obtained by integrating the corresponding injection peaks—were normalized for ligand concentration and corrected for dilution heats. Non-linear regression fit to a single set of sites model provided the stoichiometry of binding N, equilibrium association constant Ka, and enthalpy change ΔH for each experiment.⁵⁵

In Vivo Drug Formulation. NU223612 and NU226211 were administered intraperitoneally (ip). Compounds were suspended in 10% of total volume DMSO and 10% of total volume ethanol, followed by sonication for 1 min and vortexing for 30 s. 70% of the total volume PEG300 was added, followed by 2% of the total volume Tween80, and the solution was vortexed for 30 s. Finally, 2-hydroxypropyl- β -cyclodextrin (HP- β -CD) solution (10% aqueous solution) was added to a final concentration of 8% in a drop-wise manner. The final formulation was vortexed for 30 s to obtain a clear solution, and drugs were made once per week and stored in the dark at room temperature.

In Vivo Toxicity. To study toxicity, 8 week old male wild-type C57BL/6 mice ($n = 3$ /group) were treated with either NU223612 or NU223618 at 10, 25, 50 mg/kg, or 100 mg/kg for 3 weeks during Monday–Friday and monitored for survival, changes in physical appearance, and body weight measurements twice per week. After 3 weeks of treatment, mouse serum and brain tissue were collected and analyzed by LC/MS/MS analysis to determine IDO1-PROTAC and IDO1 enzyme inhibitor levels.

Distribution and PK. To study PK, 8 week old male wild-type C57BL/6 mice were treated with NU223612 at 25 mg/kg, followed by plasma and tissue collection at 0, 0.25, 0.5, 1, 2, 6, 8, 12, and 24 h. 5 μ L of plasma was directly loaded into a 96-well Millipore Multiscreen Solvinter 0.45 μ m low-binding PTFE hydrophilic filter plate. Brain and other tissue samples were homogenized with a 3x water dilution, and then 10 μ L was loaded into the filter plate. All plasma and tissue samples were treated with 75 μ L of 90/10 acetonitrile/water with carbamazepine as the internal standard (IS) to extract the analyte and precipitate protein. The plates were agitated on ice for approximately 10 min prior to centrifugation into a collection plate. Separate standard curves were prepared in blank mouse plasma and tissue homogenate and processed in parallel with the samples. The filtrate was directly analyzed by LC/MS/MS to determine the levels of IDO1-PROTAC. HPLC and MS/MS parameters are provided in the Supporting Information.

Survival Studies. For survival analysis, 8 week old C57BL/6 mice were intracranially (ic.) injected with 5×10^3 GL261 luciferase-modified (GL261-luc.) cells in 2.5 μ L PBS as described by.³³ At 14 days post-intracranial injection, mice were randomly assigned to two treatment groups that received: (i) vehicle control or (ii) IDO1-PROTAC (NU223612; 25 mg/kg once per day) Monday through Friday for up to 3 weeks.

Statistical Analysis. Statistical analyses were performed with GraphPad Prism 9.0 software by using Student's unpaired *t*-test. Data are represented as \pm SEM. For estimation of half-maximal degradation concentrations (DC₅₀) in U87 and GBM-43 cells, the amount of IDO protein degraded was calculated by densitometric analysis (ImageJ software) of signal intensities of IDO1 protein from western blots at

each concentration and normalized to the expression of GAPDH. The degradation percentage of IFN γ -treated samples was set to zero and was used to calibrate the protein degradation in samples treated at various concentrations of IDO1-PROTAC (NU223612). The percent protein degradation values at individual concentrations from three independent experiments were further computed using a nonlinear regression model (GraphPad Prism) to generate a sigmoidal curve and a DC₅₀ value. For overall survival analysis, survival curves were plotted using the Kaplan–Meier method and compared by log-rank (Mantel–Cox) test for significant survival benefit between treatment groups using Prism 9.3.1 software (GraphPad). Overall survival was defined as the day of tumor cell engraftment until reaching endpoint criteria and/or death. A value of $P < 0.05$ was considered to have a significant survival benefit between the two groups.

■ ASSOCIATED CONTENT

Supporting Information

The Supporting Information is available free of charge at <https://pubs.acs.org/doi/10.1021/acs.jmedchem.2c00771>.

Molecular formula SMILES notation of all compounds and their percent IDO1 degradation (CSV)

Cell lines used and growth media; antibodies used and their dilutions; screening of PROTAC library compounds in U87 and other cancer cell lines; degradation of ectopic IDO1 and enzyme-null IDO1; inhibition of IDO1 enzymatic activity by PROTACs; isothermal calorimetry binding measurement of PROTAC 3612 binding to IDO1; 3612 inhibition of non-enzyme activity of IDO1; survival of mice treated with 3612 and tissue distribution of 3612; effects of 3612 on the IDO1 and IDO2 mRNA expression in GL261 cells; analytical ¹H -NMR, ¹³C -NMR, and HPLC spectra of compounds 3612, 3618, and 6211; mass spectrometry parameters used for bioanalysis of 3612 in mouse brain and plasma; and synthetic procedures and analytical data for all IDO1 PROTACs prepared (PDF)

■ AUTHOR INFORMATION

Corresponding Authors

Gary E. Schiltz – Department of Chemistry, Northwestern University, Evanston, Illinois 60208, United States; Robert H. Lurie Comprehensive Cancer Center, Chicago, Illinois 60611, United States; Department of Pharmacology, Northwestern University Feinberg School of Medicine, Chicago, Illinois 60611, United States; orcid.org/0000-0003-4180-5051; Email: gary-schiltz@northwestern.edu

Derek A. Wainwright – Department of Neurological Surgery and Department of Medicine—Division of Hematology and Oncology, Northwestern University Feinberg School of Medicine, Chicago, Illinois 60611, United States; Robert H. Lurie Comprehensive Cancer Center, Chicago, Illinois 60611, United States; Department of Microbiology-Immunology, Northwestern University Feinberg School of Medicine, Chicago, Illinois 60611, United States; orcid.org/0000-0001-7232-4264; Email: Derekwainwright@northwestern.edu

Authors

Lakshmi R. Bollu – Department of Neurological Surgery, Northwestern University Feinberg School of Medicine, Chicago, Illinois 60611, United States

Prashant V. Bommi – Department of Neurological Surgery, Northwestern University Feinberg School of Medicine, Chicago, Illinois 60611, United States

Paige J. Monsen – Department of Chemistry, Northwestern University, Evanston, Illinois 60208, United States

Lijie Zhai – Department of Neurological Surgery, Northwestern University Feinberg School of Medicine, Chicago, Illinois 60611, United States

Kristen L. Lauing – Department of Neurological Surgery, Northwestern University Feinberg School of Medicine, Chicago, Illinois 60611, United States

April Bell – Department of Neurological Surgery, Northwestern University Feinberg School of Medicine, Chicago, Illinois 60611, United States

Miri Kim – Department of Neurological Surgery, Loyola University Medical Center, Maywood, Illinois 60153, United States

Erik Ladomersky – Department of Neurological Surgery, Northwestern University Feinberg School of Medicine, Chicago, Illinois 60611, United States

Xinyu Yang – WuXi AppTec, Shanghai 200131, People's Republic of China

Leonidas C. Platanias – Department of Medicine—Division of Hematology and Oncology, Northwestern University Feinberg School of Medicine, Chicago, Illinois 60611, United States; Robert H. Lurie Comprehensive Cancer Center, Chicago, Illinois 60611, United States

Daniela E. Matei – Robert H. Lurie Comprehensive Cancer Center, Chicago, Illinois 60611, United States; Department of Obstetrics and Gynecology, Northwestern University Feinberg School of Medicine, Chicago, Illinois 60611, United States

Marcelo G. Bonini – Department of Medicine—Division of Hematology and Oncology, Northwestern University Feinberg School of Medicine, Chicago, Illinois 60611, United States; Robert H. Lurie Comprehensive Cancer Center, Chicago, Illinois 60611, United States

Hidayatullah G. Munshi – Department of Medicine—Division of Hematology and Oncology, Northwestern University Feinberg School of Medicine, Chicago, Illinois 60611, United States; Robert H. Lurie Comprehensive Cancer Center, Chicago, Illinois 60611, United States

Rintaro Hashizume – Robert H. Lurie Comprehensive Cancer Center, Chicago, Illinois 60611, United States; Department of Pediatrics – Division of Hematology, Oncology, and Stem Cell Transplantation, Northwestern University Feinberg School of Medicine, Chicago, Illinois 60611, United States

Jennifer D. Wu – Robert H. Lurie Comprehensive Cancer Center, Chicago, Illinois 60611, United States; Department of Urology, Northwestern University Feinberg School of Medicine, Chicago, Illinois 60611, United States; Department of Microbiology-Immunology, Northwestern University Feinberg School of Medicine, Chicago, Illinois 60611, United States

Bin Zhang – Department of Medicine—Division of Hematology and Oncology, Northwestern University Feinberg School of Medicine, Chicago, Illinois 60611, United States; Department of Microbiology-Immunology, Northwestern University Feinberg School of Medicine, Chicago, Illinois 60611, United States; orcid.org/0000-0002-6631-7647

Charles David James – Department of Neurological Surgery, Northwestern University Feinberg School of Medicine, Chicago, Illinois 60611, United States

Peiwen Chen – Department of Neurological Surgery, Northwestern University Feinberg School of Medicine, Chicago, Illinois 60611, United States

Masha Kocherginsky – Robert H. Lurie Comprehensive Cancer Center, Chicago, Illinois 60611, United States; Department of

Obstetrics and Gynecology and Department of Preventive Medicine, Northwestern University Feinberg School of Medicine, Chicago, Illinois 60611, United States

Craig Horbinski – Department of Neurological Surgery and Department of Pathology, Northwestern University Feinberg School of Medicine, Chicago, Illinois 60611, United States; Robert H. Lurie Comprehensive Cancer Center, Chicago, Illinois 60611, United States

Michael D. Cameron – Department of Molecular Therapeutics, The Scripps Research Institute, Scripps Florida, Jupiter, Florida 33458, United States; orcid.org/0000-0003-3154-4775

Arabela A. Grigorescu – Department of Molecular Biosciences, Northwestern University Weinberg College of Arts and Sciences, Evanston, Illinois 60208, United States

Bakhtiar Yamini – Department of Neurological Surgery, Division of the Biological Sciences, The University of Chicago, Chicago, Illinois 60637, United States

Rimas V. Lukas – Robert H. Lurie Comprehensive Cancer Center, Chicago, Illinois 60611, United States; Department of Neurology, Northwestern University Feinberg School of Medicine, Chicago, Illinois 60611, United States

Complete contact information is available at:

<https://pubs.acs.org/10.1021/acs.jmedchem.2c00771>

Author Contributions

● L.R.B. and P.V.B. contributed equally. Conception and design: L.R.B., D.A.W., G.E.S.; development of methodology: L.R.B., E.R.L., A.A.G., K.L.L., G.E.S., D.A.W.; acquisition of data: L.R.B., P.V.B., P.J.M.; analysis and interpretation of data: L.R.B., P.V.B., G.E.S., D.A.W.; writing, review, and/or revision of the manuscript: L.R.B., P.V.B., L.Z., R.V.L., G.E.S., P.J.M., D.A.W.; administrative, technical, or material support: L.C.P., D.E.M., M.G.B., H.G.M., R.H., J.D.W., B.Z., C.D.J., M.D.C., A.A.G.; study supervision: G.E.S., D.A.W. The manuscript was written through the contributions of all authors. All authors critically read and intellectually contributed to the manuscript.

Notes

The authors declare the following competing financial interest(s): Dr. Lukas has received honoraria for serving on a Scientific Advisory Board for Merck, and honoraria for serving on the Speakers Bureau for Novocure. He has received research support for drug only use from BMS. Findings regarding the potential applications of the IDO1-PROTACs described herein are the subject of U.S. patent application 17/305,311, filed July 2, 2021, owned by Northwestern University and lists D.A.W. and G.E.S. as inventors.

ACKNOWLEDGMENTS

We thank and acknowledge WuXi AppTec (China) for technical assistance with compound synthesis. This work was supported in part by the National Institutes of Health (NIH) grants R01NS113425 (L.C.P.), R01NS102669 (C.H.), P50CA221747 (L.C.P., R.V.L., C.H., C.D.J., and D.A.W.), R01NS097851 (D.A.W. and G.E.S.), K02AG068617 (D.A.W.), BrainUp grant 2136 (R.V.L. and D.A.W.), Lou Malnati Brain Tumor Institute (R.V.L., G.E.S., and D.A.W.), American Cancer Scholar Research Scholar Award RSG-21-058-01 - CCE (D.A.W.), the GBM Foundation (D.A.W.), 5 for the Fight (D.A.W.), and the Chicago Biomedical Consortium Director's Fund Award DF-008 (G.E.S., D.A.W.).

■ ABBREVIATIONS USED

AR2G, amine reactive second generation; BBB, blood-brain barrier; BLI, biolayer interferometry; CRBN, cereblon; DIPG, diffuse intrinsic pontine glioma; GAPDH, glyceraldehyde phosphate dehydrogenase; GBM, glioblastoma; ICB, immune checkpoint blockade; IDO1, indoleamine 2,3-dioxygenase 1; IFN γ , interferon gamma; ITC, isothermal titration calorimetry; Kyn, kynurenine; NF- κ B, nuclear factor kappa B; NU223618, BMS-986205 (linrodostat); PBMC, peripheral blood mononuclear cell; PD, pharmacodynamic; PEG, polyethylene glycol; PK, pharmacokinetic; PPI, protein-protein interaction; PRO-TAC, proteolysis targeting chimera; SAR, structure-activity relationship; TDO, tryptophan dioxygenase; Treg, regulatory T cell; Trp, tryptophan; VHL, Von Hippel-Lindau

■ REFERENCES

- (1) Lukas, R. V.; Wainwright, D. A.; Ladomersky, E.; Sachdev, S.; Sonabend, A. M.; Stupp, R. Newly Diagnosed Glioblastoma: A Review on Clinical Management. *Oncology (Williston Park)* **2019**, *33*, 91–100.
- (2) Stupp, R.; Taillibert, S.; Kanner, A.; Read, W.; Steinberg, D.; Lhermitte, B.; Toms, S.; Idbaih, A.; Ahluwalia, M. S.; Fink, K.; Di Meco, F.; Lieberman, F.; Zhu, J. J.; Stragliotto, G.; Tran, D.; Brem, S.; Hottinger, A.; Kirson, E. D.; Lavy-Shahaf, G.; Weinberg, U.; Kim, C. Y.; Paek, S. H.; Nicholas, G.; Bruna, J.; Hirte, H.; Weller, M.; Palti, Y.; Hegi, M. E.; Ram, Z. Effect of Tumor-Treating Fields Plus Maintenance Temozolomide vs Maintenance Temozolomide Alone on Survival in Patients With Glioblastoma: A Randomized Clinical Trial. *JAMA* **2017**, *318*, 2306–2316.
- (3) Reardon, D. A.; Brandes, A. A.; Omuro, A.; Mulholland, P.; Lim, M.; Wick, A.; Baehring, J.; Ahluwalia, M. S.; Roth, P.; Bähr, O.; Phuphanich, S.; Sepulveda, J. M.; De Souza, P.; Sahebjam, S.; Carleton, M.; Tatsuoka, K.; Taitt, C.; Zwirter, R.; Sampson, J.; Weller, M. Effect of Nivolumab vs Bevacizumab in Patients With Recurrent Glioblastoma: The CheckMate 143 Phase 3 Randomized Clinical Trial. *JAMA Oncol* **2020**, *6*, 1003–1010.
- (4) Chan, H. Y.; Choi, J.; Jackson, C.; Lim, M. Combination immunotherapy strategies for glioblastoma. *J Neurooncol* **2021**, *151*, 375–391.
- (5) Weller, M.; Lim, M.; Idbaih, A.; Steinbach, J.; Finocchiaro, G.; Raval, R.; Ashby, L.; Ansstas, G.; Baehring, J.; Taylor, J.; Honnorat, J.; Petrecca, K.; de Vos, F.; Wick, A.; Sumrall, A.; Roberts, M.; Slepets, R.; Warad, D.; Lee, M.; Reardon, D.; Omuro, A. CTIM-25. A RANDOMIZED PHASE 3 STUDY OF NIVOLUMAB OR PLACEBO COMBINED WITH RADIOTHERAPY PLUS TEMOZOLOMIDE IN PATIENTS WITH NEWLY DIAGNOSED GLIOBLASTOMA WITH METHYLATED MGMT PROMOTER: CHECKMATE 548. *Neuro-Oncology* **2021**, *23*, vi55–vi56.
- (6) Bristol-Myers Squibb. *Bristol-myers squibb announces phase 3 checkmate -498 study did not meet primary endpoint of overall survival with opdivo (nivolumab) plus radiation in patients with newly diagnosed mgmt- unmethylated glioblastoma multiforme*. 2019, (accessed on May 09, 2019); Available from: <https://news.bms.com/news/corporate-financial/2019/Bristol-Myers-Squibb-Announces-Phase-3-CheckMate--498-Study-Did-Not-Meet-Primary-Endpoint-of-Overall-Survival-with-Opdivo-nivolumab-Plus-Radiation-in-Patients-with-Newly-Diagnosed-MGMT-Unmethylated-Glioblastoma-Multiforme/default.aspx>.
- (7) Wainwright, D. A.; Dey, M.; Chang, A.; Lesniak, M. S. Targeting Tregs in Malignant Brain Cancer: Overcoming IDO. *Front Immunol* **2013**, *4*, 116.
- (8) Zhai, L.; Lauing, K. L.; Chang, A. L.; Dey, M.; Qian, J.; Cheng, Y.; Lesniak, M. S.; Wainwright, D. A. The role of IDO in brain tumor immunotherapy. *J Neurooncol* **2015**, *123*, 395–403.
- (9) Zhai, L.; Ladomersky, E.; Lenzen, A.; Nguyen, B.; Patel, R.; Lauing, K. L.; Wu, M.; Wainwright, D. A. IDO1 in cancer: a Gemini of immune checkpoints. *Cell Mol Immunol* **2018**, *15*, 447–457.
- (10) Zhai, L.; Spranger, S.; Binder, D. C.; Gritsina, G.; Lauing, K. L.; Giles, F. J.; Wainwright, D. A. Molecular Pathways: Targeting IDO1 and Other Tryptophan Dioxygenases for Cancer Immunotherapy. *Clin. Cancer Res.* **2015**, *21*, 5427–5433.
- (11) Wainwright, D. A.; Balyasnikova, I. V.; Chang, A. L.; Ahmed, A. U.; Moon, K. S.; Auffinger, B.; Tobias, A. L.; Han, Y.; Lesniak, M. S. IDO expression in brain tumors increases the recruitment of regulatory T cells and negatively impacts survival. *Clin. Cancer Res.* **2012**, *18*, 6110–6121.
- (12) Zhai, L.; Ladomersky, E.; Lauing, K. L.; Wu, M.; Genet, M.; Gritsina, G.; Györfy, B.; Brastianos, P. K.; Binder, D. C.; Sosman, J. A.; Giles, F. J.; James, C. D.; Horbinski, C.; Stupp, R.; Wainwright, D. A. Infiltrating T Cells Increase IDO1 Expression in Glioblastoma and Contribute to Decreased Patient Survival. *Clin. Cancer Res.* **2017**, *23*, 6650–6660.
- (13) Rosenberg, A. J.; Wainwright, D. A.; Rademaker, A.; Galvez, C.; Genet, M.; Zhai, L.; Lauing, K. L.; Mulcahy, M. F.; Hayes, J. P.; Odell, D. D.; Horbinski, C.; Komanduri, S.; Tetreault, M. P.; Kim, K. A.; Villalor, V. M. Indoleamine 2,3-dioxygenase 1 and overall survival of patients diagnosed with esophageal cancer. *Oncotarget* **2018**, *9*, 23482–23493.
- (14) Wang, W.; Huang, L.; Jin, J. Y.; Pi, W.; Ellsworth, S. G.; Jolly, S.; Mellor, A. L.; Machtay, M.; Kong, F. S. A Validation Study on IDO Immune Biomarkers for Survival Prediction in Non-Small Cell Lung Cancer: Radiation Dose Fractionation Effect in Early-Stage Disease. *Clin. Cancer Res.* **2020**, *26*, 282–289.
- (15) Inaba, T.; Ino, K.; Kajiyama, H.; Yamamoto, E.; Shibata, K.; Nawa, A.; Nagasaka, T.; Akimoto, H.; Takikawa, O.; Kikkawa, F. Role of the immunosuppressive enzyme indoleamine 2,3-dioxygenase in the progression of ovarian carcinoma. *Gynecol Oncol* **2009**, *115*, 185–192.
- (16) Mangaonkar, A.; Mondal, A. K.; Fulzule, S.; Pundkar, C.; Park, E. J.; Jillella, A.; Kota, V.; Xu, H.; Savage, N. M.; Shi, H.; Munn, D.; Kolhe, R. A novel immunohistochemical score to predict early mortality in acute myeloid leukemia patients based on indoleamine 2,3 dioxygenase expression. *Sci. Rep.* **2017**, *7*, 12892.
- (17) Zhai, L.; Bell, A.; Ladomersky, E.; Lauing, K. L.; Bollu, L.; Nguyen, B.; Genet, M.; Kim, M.; Chen, P.; Mi, X.; Wu, J. D.; Schipma, M. J.; Wray, B.; Griffiths, J.; Unwin, R. D.; Clark, S. J.; Acharya, R.; Bao, R.; Horbinski, C.; Lukas, R. V.; Schiltz, G. E.; Wainwright, D. A. Tumor cell IDO enhances immune suppression and decreases survival independent of tryptophan metabolism in glioblastoma. *Clin. Cancer Res.* **2021**, *27*, 6514–6528.
- (18) Wainwright, D. A.; Sengupta, S.; Han, Y.; Lesniak, M. S. Thymus-derived rather than tumor-induced regulatory T cells predominate in brain tumors. *Neuro Oncol* **2011**, *13*, 1308–1323.
- (19) Wainwright, D. A.; Chang, A. L.; Dey, M.; Balyasnikova, I. V.; Kim, C. K.; Tobias, A.; Cheng, Y.; Kim, J. W.; Qiao, J.; Zhang, L.; Han, Y.; Lesniak, M. S. Durable therapeutic efficacy utilizing combinatorial blockade against IDO, CTLA-4, and PD-L1 in mice with brain tumors. *Clin. Cancer Res.* **2014**, *20*, 5290–5301.
- (20) Zhai, L.; Bell, A.; Ladomersky, E.; Lauing, K. L.; Bollu, L.; Sosman, J. A.; Zhang, B.; Wu, J. D.; Miller, S. D.; Meeks, J. J.; Lukas, R. V.; Wyatt, E.; Doglio, L.; Schiltz, G. E.; McCusker, R. H.; Wainwright, D. A. Immunosuppressive IDO in Cancer: Mechanisms of Action, Animal Models, and Targeting Strategies. *Front Immunol* **2020**, *11*, 1185.
- (21) Békés, M.; Langley, D. R.; Crews, C. M. PROTAC targeted protein degraders: the past is prologue. *Nat Rev Drug Discov* **2022**, *21*, 181–200.
- (22) Samarasinghe, K. T. G.; Crews, C. M. Targeted protein degradation: A promise for undruggable proteins. *Cell Chem Biol* **2021**, *28*, 934–951.
- (23) Sakamoto, K. M.; Kim, K. B.; Kumagai, A.; Mercurio, F.; Crews, C. M.; Deshaies, R. J. Protacs: chimeric molecules that target proteins to the Skp1-Cullin-F box complex for ubiquitination and degradation. *Proc Natl Acad Sci U S A* **2001**, *98*, 8554–8559.
- (24) Nelp, M. T.; Kates, P. A.; Hunt, J. T.; Newitt, J. A.; Balog, A.; Maley, D.; Zhu, X.; Abell, L.; Allentoff, A.; Borzilleri, R.; Lewis, H. A.; Lin, Z.; Seitz, S. P.; Yan, C.; Groves, J. T. Immune-modulating enzyme

indoleamine 2,3-dioxygenase is effectively inhibited by targeting its apo-form. *Proc Natl Acad Sci U S A* **2018**, *115*, 3249–3254.

(25) Soares, P.; Gadd, M. S.; Frost, J.; Galdeano, C.; Ellis, L.; Epemolu, O.; Rocha, S.; Read, K. D.; Ciulli, A. Group-Based Optimization of Potent and Cell-Active Inhibitors of the von Hippel-Lindau (VHL) E3 Ubiquitin Ligase: Structure-Activity Relationships Leading to the Chemical Probe (2S,4R)-1-((S)-2-(1-Cyanocyclopropanecarboxamido)-3,3-dimethylbutanoyl)-4-hydroxy-N-(4-(4-methylthiazol-5-yl)benzyl)pyrrolidine-2-carboxamide (VH298). *J. Med. Chem.* **2018**, *61*, 599–618.

(26) Edmondson, S. D.; Yang, B. C.; Fallan, C. Proteolysis targeting chimeras (PROTACs) in 'beyond rule-of-five' chemical space: Recent progress and future challenges. *Bioorg. Med. Chem. Lett.* **2019**, *29*, 1555–1564.

(27) Troup, R. L.; Fallan, C.; Baud, M. G. Current strategies for the design of PROTAC linkers: a critical review. *Exploration of Targeted Anti-tumor Therapy* **2020**, *1*, 273–312.

(28) Nowak, R. P.; DeAngelo, S. L.; Buckley, D.; He, Z.; Donovan, K. A.; An, J.; Safaei, N.; Jedrychowski, M. P.; Ponthier, C. M.; Ishoey, M.; Zhang, T.; Mancias, J. D.; Gray, N. S.; Bradner, J. E.; Fischer, E. S. Plasticity in binding confers selectivity in ligand-induced protein degradation. *Nat. Chem. Biol.* **2018**, *14*, 706–714.

(29) Hu, M.; Zhou, W.; Wang, Y.; Yao, D.; Ye, T.; Yao, Y.; Chen, B.; Liu, G.; Yang, X.; Wang, W.; Xie, Y. Discovery of the first potent proteolysis targeting chimera (PROTAC) degrader of indoleamine 2,3-dioxygenase 1. *Acta Pharm Sin B* **2020**, *10*, 1943–1953.

(30) Wu, Y.; Duan, Q.; Zou, Y.; Zhu, Q.; Xu, Y. Discovery of novel IDO1 inhibitors targeting the protein's apo form through scaffold hopping from holo-IDO1 inhibitor. *Bioorg. Med. Chem. Lett.* **2021**, *52*, 128373.

(31) Ladomersky, E.; Zhai, L.; Lenzen, A.; Lauing, K. L.; Qian, J.; Scholtens, D. M.; Gritsina, G.; Sun, X.; Liu, Y.; Yu, F.; Gong, W.; Liu, Y.; Jiang, B.; Tang, T.; Patel, R.; Platanius, L. C.; James, C. D.; Stupp, R.; Lukas, R. V.; Binder, D. C.; Wainwright, D. A. IDO1 Inhibition Synergizes with Radiation and PD-1 Blockade to Durably Increase Survival Against Advanced Glioblastoma. *Clin. Cancer Res.* **2018**, *24*, 2559–2573.

(32) Chung, D. J.; Rossi, M.; Romano, E.; Ghith, J.; Yuan, J.; Munn, D. H.; Young, J. W. Indoleamine 2,3-dioxygenase-expressing mature human monocyte-derived dendritic cells expand potent autologous regulatory T cells. *Blood* **2009**, *114*, 555–563.

(33) Opitz, C. A.; Litzemberger, U. M.; Sahm, F.; Ott, M.; Tritschler, I.; Trump, S.; Schumacher, T.; Jestaedt, L.; Schrenk, D.; Weller, M.; Jugold, M.; Guillemin, G. J.; Miller, C. L.; Lutz, C.; Radlwimmer, B.; Lehmann, I.; von Deimling, A.; Wick, W.; Platten, M. An endogenous tumour-promoting ligand of the human aryl hydrocarbon receptor. *Nature* **2011**, *478*, 197–203.

(34) Ladomersky, E.; Zhai, L.; Lauing, K. L.; Bell, A.; Xu, J.; Kocherginsky, M.; Zhang, B.; Wu, J. D.; Podojil, J. R.; Platanius, L. C.; Mochizuki, A. Y.; Prins, R. M.; Kumthekar, P.; Raizer, J.; Dixit, K.; Lukas, R. V.; Horbinski, C.; Wei, M.; Zhou, C.; Pawelec, G.; Campisi, J.; Grohmann, U.; Prendergast, G. C.; Munn, D.; Wainwright, D. A. Advanced Age Increases Immunosuppression in the Brain and Decreases Immunotherapeutic Efficacy in Subjects with Glioblastoma. *Clin. Cancer Res.* **2020**, *26*, 5232–5245.

(35) Concepcion, J.; Witte, K.; Wartchow, C.; Choo, S.; Yao, D.; Persson, H.; Wei, J.; Li, P.; Heidecker, B.; Ma, W.; Varma, R.; Zhao, L. S.; Perillat, D.; Carricato, G.; Recknor, M.; Du, K.; Ho, H.; Ellis, T.; Gamez, J.; Howes, M.; Phi-Wilson, J.; Lockard, S.; Zuk, R.; Tan, H. Label-free detection of biomolecular interactions using BioLayer interferometry for kinetic characterization. *Comb Chem High Throughput Screen* **2009**, *12*, 791–800.

(36) Liu, X.; Zhang, X.; Lv, D.; Yuan, Y.; Zheng, G.; Zhou, D. Assays and technologies for developing proteolysis targeting chimera degraders. *Future Med. Chem.* **2020**, *12*, 1155–1179.

(37) Roy, M. J.; Winkler, S.; Hughes, S. J.; Whitworth, C.; Galant, M.; Farnaby, W.; Rumpel, K.; Ciulli, A. SPR-Measured Dissociation Kinetics of PROTAC Ternary Complexes Influence Target Degradation Rate. *ACS Chem. Biol.* **2019**, *14*, 361–368.

(38) Hughes, S. J.; Ciulli, A. Molecular recognition of ternary complexes: a new dimension in the structure-guided design of chemical degraders. *Essays Biochem.* **2017**, *61*, 505–516.

(39) Zhai, L.; Ladomersky, E.; Dostal, C. R.; Lauing, K. L.; Swoap, K.; Billingham, L. K.; Gritsina, G.; Wu, M.; McCusker, R. H.; Binder, D. C.; Wainwright, D. A. Non-tumor cell IDO1 predominantly contributes to enzyme activity and response to CTLA-4/PD-L1 inhibition in mouse glioblastoma. *Brain Behav Immun* **2017**, *62*, 24–29.

(40) Pallotta, M. T.; Orabona, C.; Volpi, C.; Vacca, C.; Belladonna, M. L.; Bianchi, R.; Servillo, G.; Brunacci, C.; Calvitti, M.; Biciato, S.; Mazza, E. M.; Boon, L.; Grassi, F.; Fioretti, M. C.; Fallarino, F.; Puccetti, P.; Grohmann, U. Indoleamine 2,3-dioxygenase is a signaling protein in long-term tolerance by dendritic cells. *Nat. Immunol.* **2011**, *12*, 870–878.

(41) Uyttenhove, C.; Pilotte, L.; Théate, I.; Stroobant, V.; Colau, D.; Parmentier, N.; Boon, T.; Van den Eynde, B. J. Evidence for a tumoral immune resistance mechanism based on tryptophan degradation by indoleamine 2,3-dioxygenase. *Nat Med* **2003**, *9*, 1269–1274.

(42) Long, G. V.; Dummer, R.; Hamid, O.; Gajewski, T. F.; Caglevic, C.; Dalle, S.; Arance, A.; Carlino, M. S.; Grob, J. J.; Kim, T. M.; Demidov, L.; Robert, C.; Larkin, J.; Anderson, J. R.; Maleski, J.; Jones, M.; Diede, S. J.; Mitchell, T. C. Epcadostat plus pembrolizumab versus placebo plus pembrolizumab in patients with unresectable or metastatic melanoma (ECHO-301/KEYNOTE-252): a phase 3, randomised, double-blind study. *Lancet Oncol* **2019**, *20*, 1083–1097.

(43) Zhang, Y.; Bowman, K.; Maleski, J.; Diamond, S.; Yeleswaram, S. Effects of Epcadostat on Brain Extracellular Fluid Concentrations of Serotonin-an Intracerebral Microdialysis Study in Sprague-Dawley Rats. *Drug Metab. Dispos.* **2019**, *47*, 710–714.

(44) Odunsi, K.; Qian, F.; Lugade, A. A.; Yu, H.; Geller, M. A.; Fling, S. P.; Kaiser, J. C.; Lacroix, A. M.; D'Amico, L.; Ramchurren, N.; Morishima, C.; Disis, M. L.; Dennis, L.; Danaher, P.; Warren, S.; Nguyen, V. A.; Ravi, S.; Tsuji, T.; Rosario, S.; Zha, W.; Hutson, A.; Liu, S.; Lele, S.; Zsiros, E.; McGray, A. J. R.; Chiello, J.; Koya, R.; Chodon, T.; Morrison, C. D.; Putluri, V.; Putluri, N.; Mager, D. E.; Gunawan, R.; Cheever, M. A.; Battaglia, S.; Matsuzaki, J. Metabolic adaptation of ovarian tumors in patients treated with an IDO1 inhibitor constrains antitumor immune responses. *Sci Transl Med* **2022**, *14*, No. eabg8402.

(45) Löb, S.; Königsgrainer, A.; Zieker, D.; Brücher, B. L.; Rammensee, H. G.; Opelz, G.; Terness, P. IDO1 and IDO2 are expressed in human tumors: levo- but not dextro-1-methyl tryptophan inhibits tryptophan catabolism. *Cancer Immunol Immunother* **2009**, *58*, 153–157.

(46) Grivennikov, S. I.; Karin, M. Dangerous liaisons: STAT3 and NF-kappaB collaboration and crosstalk in cancer. *Cytokine Growth Factor Rev.* **2010**, *21*, 11–19.

(47) Bonizzi, G.; Karin, M. The two NF-kappaB activation pathways and their role in innate and adaptive immunity. *Trends Immunol.* **2004**, *25*, 280–288.

(48) Ladomersky, E.; Scholtens, D. M.; Kocherginsky, M.; Hibler, E. A.; Bartom, E. T.; Otto-Meyer, S.; Zhai, L.; Lauing, K. L.; Choi, J.; Sosman, J. A.; Wu, J. D.; Zhang, B.; Lukas, R. V.; Wainwright, D. A. The Coincidence Between Increasing Age, Immunosuppression, and the Incidence of Patients With Glioblastoma. *Front Pharmacol* **2019**, *10*, 200.

(49) Fraunhofer, K. J.; DelMonte, A. J.; Beutner, G. L.; Bultman, M. S.; Camacho, K.; Cohen, B.; Dixon, D. D.; Fan, Y.; Fanfair, D.; Freitag, A. J.; Glace, A. W.; Gonzalez-Bobes, F.; Gujjar, M.; Haley, M. W.; Hickey, M. R.; Ho, J.; Iyer, V.; Maity, P.; Patel, S.; Rosso, V. W.; Schmidt, M. A.; Stevens, J. M.; Tan, Y.; Wilbert, C.; Young, I. S.; Yu, M. Rapid Development of a Commercial Process for Linrodostat, an Indoleamine 2,3-Dioxygenase (IDO) Inhibitor. *Org. Process Res. Dev.* **2019**, *23*, 2482–2498.

(50) Bertuzzi, G.; Locatelli, E.; Colecchia, D.; Calandro, P.; Bonini, B. F.; Chandanshive, J. Z.; Mazzanti, A.; Zani, P.; Chiariello, M.; Comes Franchini, M. Straightforward synthesis of a novel ring-fused pyrazole-lactam and in vitro cytotoxic activity on cancer cell lines. *Eur. J. Med. Chem.* **2016**, *117*, 1–7.

(51) Li, Z.; Pinch, B. J.; Olson, C. M.; Donovan, K. A.; Nowak, R. P.; Mills, C. E.; Scott, D. A.; Doctor, Z. M.; Eleuteri, N. A.; Chung, M.;

Sorger, P. K.; Fischer, E. S.; Gray, N. S. Development and Characterization of a Wee1 Kinase Degradar. *Cell Chem Biol* **2020**, *27*, 57–65 e9.

(52) Bommi, P. V.; Chand, V.; Mukhopadhyay, N. K.; Raychaudhuri, P.; Bagchi, S. NER-factor DDB2 regulates HIF1alpha and hypoxia-response genes in HNSCC. *Oncogene* **2020**, *39*, 1784–1796.

(53) Zhai, L.; Ladomersky, E.; Bell, A.; Dussold, C.; Cardoza, K.; Qian, J.; Lauing, K. L.; Wainwright, D. A. Quantification of IDO1 enzyme activity in normal and malignant tissues. *Methods Enzymol.* **2019**, *629*, 235–256.

(54) Biltonen, R. L.; Langerman, N. Microcalorimetry for biological chemistry: experimental design, data analysis, and interpretation. *Methods Enzymol.* **1979**, *61*, 287–318.

(55) Privalov, P. L.; Dragan, A. I. Microcalorimetry of biological macromolecules. *Biophys. Chem.* **2007**, *126*, 16–24.